The chemical dynamics of hydrogen/hydrogen peroxide blends diluted with steam at compression ignition relevant conditions

Efstathios-Al. Tingas

School of Engineering and the Built Environment, Edinburgh Napier University, Edinburgh EH10 5DT, United Kingdom

Abstract

In the current work, the use of hydrogen peroxide as an additive to hydrogen/air mixtures is proposed and explored computationally, in conditions relevant to compression ignition engines. The hydrogen/hydrogen peroxide blends are supplemented with steam for NOx emissions reduction purposes.

The objective of the current work is to explore fundamental aspects of the proposed technology, with an emphasis on identifying the key chemical pathways that control the ignition delay time and NOx emissions, using mathematical tools from the computational singular perturbation (CSP) approach.

The proposed technology demonstrates a noteworthy potential for use in CI engines, since a 10% (per fuel volume) addition of hydrogen peroxide decreases the ignition delay time to 1 ms, while the mass fraction of NO in equilibrium drops by 100%. Reactions H + O_2 → OH + O and H + O_2 (+M) → HO_2 (+M) play key roles in the acceleration of the ignition delay time, while the thermal and the NNH mechanisms are identified as the dominant pathways for the production of NO. A further 12% addition of steam (per mixture's volume) induces a two orders of magnitude drop to NO emissions and slightly increases the ignition delay time by 8%. Finally, at sufficiently high steam addition conditions (in the region of 30% and above by mixture's volume), the system exhibits two stage ignition (mainly owed to reaction HO_2 + OH → H_2O + O_2), a phe-

Email address: e.tingas@napier.ac.uk (Efstathios-Al. Tingas)

nomenon that is unique, considering that the initial mixture includes solely hydrogen-based chemical species.

Keywords: additive, CSP, explosive dynamics, diesel engines, hydrogen, NOx

1. Introduction

Both national and international regulations originating from environmental concerns, mandate the decarbonisation of the transport sector for the most advanced economies by 2050. Electrification is meant to play a key role to this direction, however, electric vehicles (EVs) currently face significant challenges that prevent such technology from replacing the internal combustion engines (ICEs) in all different modes of transport. For instance, electrification appears to be a feasible solution for light-duty and non-commercial vehicles but for heavy-goods vehicles (HGVs), ships and airplanes, the replacement of the ICE with electric motor currently is perceived to be unrealistic. Thus, a large share of the transportation sector will need to use ICEs for many years to come [1]. Therefore, there is a need for decarbonisation of ICEs using alternative fuels.

One of the most popular alternative fuels is hydrogen, which can be created from renewable sources, thus, constituting one of the cleanest solutions (if not the cleanest) for use in ICEs. The use of hydrogen in ICEs is not new. In fact, hydrogen ICE (or H_2ICE for short) technology has been continuously developing over the last two centuries, with the first H_2ICE dating back to the 19th century [2]. The focus of this past research has primarily been on the hydrogen usage in spark ignition (SI) engines.

Therefore, there is a particularly rich scientific literature on the use of hydrogen in SI engines, which dates to many decades back. These efforts intensified and became more systematic in the 1970s, after the occurrence of the energy crisis that highlighted the importance of alternatives to fossil fuels. Over these past five decades, hydrogen combustion in SI engines has been investigated extensively both experimentally and computationally, either as a sole fuel or as

an additive, in view of a wide variety of configurations and levels of complexity [3–7].

On the other hand, the available literature for hydrogen usage in compression ignition (CI) engines is more limited [8–12]. Hydrogen use in CI engines has not been particularly attractive because of hydrogen's large resistance to ignition. As a result, the great benefits of CI against SI engines (i.e., fuel economy, power efficiency, durability and heavy-duty application) fueled with hydrogen have largely remained unexplored.

In fact, hydrogen use in CI engines has been mainly investigated in dual-fuel configurations with only few studies on pure hydrogen operation [11]. The implementation of hydrogen in a single-fuel concept has been proven to be challenging due to the high compression ratios required in order to overcome the high auto-ignition temperature. In dual-fuel operation, (where hydrogen is used along with another more reactive fuel which promotes the ignition of the mixture) hydrogen has been used with carbon-based fuels, such as diesel [13–55], biodiesel [46, 56–60], biodiesel-diesel blends [61, 62], methane-diesel blends [63, 64], methanol-diesel blends [64], biodiesel-natural gas blends [65], diesel-natural gas blends [66], biodiesel-ethanol blends [67], biodiesel-butanol blends [68], natural gas [69, 70], diethyl ether [71], jatropha oil [72, 73], neem oil methyl ester [74], lemon grass oil [75], liquefied petroleum gas [76–79], compressed natural gas [80], biogas [81] and ethanol [82]. Being carbon-based, all these fuel blends produce carbonaceous emissions (e.g., CO_2) directly or indirectly (depending how these fuels are originally produced), thus, cancelling or reducing the efforts for drastic green house gases (GHG) reduction. Limited studies have also been reported with the use of glow plug assist (e.g., [83–88]) enabling the pre-heating of the inlet air, but these studies highlighted the detrimental effect on the system's performance and efficiency along with a high risk of increased production of NOx emissions. Thus, it can be concluded that the use of hydrogen in CI engines remains an unresolved problem.

Ideally, in a dual fuel concept, the added fuel, which would enhance the system's propensity to ignition, would not be carbon-based. One such chemical

substance that has such potential is hydrogen peroxide (H_2O_2) [89]. Hydrogen peroxide has been used for many decades for propulsion purposes in aerospace applications [90–99]. Moreover, the addition of hydrogen peroxide in fuel/air mixtures for conventional transport-related applications is a well-documented method of effective ignition promotion. Injected as a pure substance or as emulsified fuel into the engine cylinder, hydrogen peroxide has been successfully tested with fuels like n-decane [100], natural gas [101, 102], methane [103–105], diesel [106–112], gasoline [113], n-heptane [114], iso-octane [115], jatropha oil [116], n-butanol [117], ethanol [118, 119], ethanol-diesel [120] and ammonia [121].

Thus, in the current work, the concept of using hydrogen with hydrogen peroxide as an additive for ignition promotion purposes is proposed and tested computationally for the first time to the best of the author's knowledge. The proposed technology can be supplemented by the addition of steam, with the purpose of NOx emissions reduction which is a well-established method for decreasing emissions. The current work aims to be the first step in developing the proposed technology which can have direct application to CI engines used for HGVs and marine transportation. It is understood though that the successful deployment of the proposed technology must also be supported by the prior appropriate logistics and lifecycle analyses of hydrogen peroxide.

As such, the current work focuses on fundamental aspects of the proposed technology, and aims to explore the effect of hydrogen peroxide addition in hydrogen/air mixtures in the context of homogeneous batch reactor simulations, in view of: (i) the ignition delay time and (ii) NOx emissions. The main focus though will be to analyse the key chemical pathways and the dominant chemical dynamics related to the ignition delay time and NOx emissions as a result of the addition of hydrogen peroxide and steam into hydrogen/air mixtures. Moreover, the conclusions will be extended to a range of initial temperatures, with the purpose of identifying trends in the changes of the pertinent key chemistry, induced by the addition of hydrogen peroxide and steam. The operating conditions that are explored in the current study aim to simulate those in CI engines. Hence, fuel lean ($\phi = 0.4$) hydrogen/air mixtures are used, for initial temperatures

ranging from 800 K to 1,000 K and initial pressures of 40 atm.

In order to accomplish the aforementioned goal of identifying the key chemical pathways, mathematical tools from the computational singular perturbation (CSP) method will be used [122]. CSP is one of the most rigorous methods for analysing highly complex multiscale systems of reacting flows, and has been successfully tested in a wide range of applications.

The structure of the paper is as follows. Firstly, a brief description of the CSP mathematical tools that are used in the main analysis is provided. For more details on the tools the reader is referred to the cited works and the works therein. The main part of the paper is split into two sections: in the first, the addition of hydrogen peroxide is discussed while in the second, the addition of steam is analysed. In each of these sections the analysis focuses on the ignition delay time and NOx emissions.

2. Methods

In the current study, the widely validated *Aramco 3* reaction mechanism was selected for the description of the hydrogen combustion [123]. The hydrogen mechanism was supplemented with the nitrogen sub-mechanism of *Glarborg et al.* [124]. A comparison of the *Aramco 3* mechanism with other modern widely validated hydrogen mechanisms is provided in the Supplementary material.

Table 1 displays the reactions that are highlighted in the analysis next. The symbols "f" and "b" used next to the reaction numbers, stand for forward and backward, respectively. The reactions listed in Table 1 are those which are identified by the various CSP tools to play a key role either to the control of the ignition delay time or to the production of NOx emissions. These reactions will be discussed in detail next.

Table 1: The most significant reactions to the dynamics of the system in all examined cases [123, 124]. The pair of reactions (13,14) and (19,20) is duplicate with different rate constants, accounting for the high and low temperature regime, respectively. In the following they will be considered as a single reaction and they will be denoted as reactions 13/14 and 19/20.

3.	$H_2 + OH \leftrightarrow H_2O + H$	19/20.	$2HO_2 \leftrightarrow H_2O_2 + O_2$
5.	$H + O_2 \leftrightarrow OH + O$	21.	$H + O_2 (+M) \leftrightarrow HO_2 (+M)$
7.	$O + H_2O \leftrightarrow 2OH$	63.	$N + NO \leftrightarrow N_2 + O$
9.	$H_2O_2 (+M) \leftrightarrow 2OH (+M)$	64.	$NNH \leftrightarrow N_2 + H$
11.	$H_2O_2 + H \leftrightarrow H_2 + HO_2$	68.	$NNH + O \leftrightarrow NH + NO$
13/14.	$H_2O_2 + OH \leftrightarrow H_2O + HO_2$	70.	$NNH + O_2 \leftrightarrow N_2 + HO_2$
18.	$HO_2 + OH \leftrightarrow H_2O + O_2$	149.	$N_2O (+M) \leftrightarrow N_2 + O (+M)$
		151.	$N_2O + O \leftrightarrow 2NO$

In the current work, tools from the computational singular perturbation (CSP) approach are used [122] for identifying the key chemical mechanisms that control the ignition delay time and the NOx emissions. These tools have been already tested successfully in a wide range of different applications in reacting flows. Here only brief descriptions of the mathematical tools will be provided, but for a detailed analysis of the CSP framework and the developed tools, the reader is referred to Refs [125–128]. In the CSP framework, the vector field of the original system of species mass fractions and temperature ordinary differential equations (ODEs) is decomposed into components, typically called modes. Therefore, the original system of Eqs. 1

$$\frac{d\boldsymbol{z}}{dt} = \boldsymbol{g}(\boldsymbol{z}) = \sum_{k=1}^{2K} \hat{\mathbf{S}}_k R^k, \tag{1}$$

is transformed to

$$\frac{d\boldsymbol{z}}{dt} = \boldsymbol{g}(\boldsymbol{z}) = \sum_{i=1}^{N+1} \boldsymbol{a}_i f^i. \tag{2}$$

In the above Eqs. 1-2, $\boldsymbol{z}$ is a column vector with $(N+1)$ solution variables including N species mass fractions ($\boldsymbol{y}$) and temperature (T), $\boldsymbol{g}(\boldsymbol{z})$ the chemical reaction source term, $\hat{\mathbf{S}}_k$ and R^k are the $(N+1)$-dimensional generalized

stoichiometric column vector and the reaction rate, respectively, of the k-th unidirectional reaction of a total of $2K$ irreversible reactions, $\boldsymbol{a}_i$ is the $(N+1)$-dimensional CSP basis column vector and $f^i{=}\boldsymbol{b}^i \cdot \boldsymbol{g}(\boldsymbol{z})$ is the related amplitude, which is produced using the dual basis row vector $\boldsymbol{b}^i$ ($\boldsymbol{b}^i \cdot \boldsymbol{a}_j = \delta^i_j$). Interested in leading order accuracy, the CSP basis vectors $\boldsymbol{a}_i$, $\boldsymbol{b}^i$ can be approximated by the right ($\boldsymbol{\alpha}_i$) and left ($\boldsymbol{\beta}^i$), respectively, eigenvectors of the Jacobian $\boldsymbol{J}$ of $\boldsymbol{g}(\boldsymbol{z})$. Each one of the CSP modes is described by a timescale (which sets the timeframe of action of the mode) and an amplitude (which determines the impact of that mode to the system's slow evolution). The timescale of each CSP mode is defined as the inverse norm of the associated eigenvalue, i.e., $\tau_i = |\lambda_i|^{-1}$, where $\lambda_i = \boldsymbol{\beta}^i \cdot \boldsymbol{J} \cdot \boldsymbol{\alpha}_i$. The mathematical tools employed in the analysis next are the following:

- the timescale participation index (TPI), which identifies the reactions mostly related to each mode's timescale [129–132]; thus, for each CSP mode, the TPIs of all reactions are calculated and the largest ones (in absolute value) are selected; when positive, the related reaction favors the explosive character of the mode's timescale, while when negative the associated reaction tends to dissipate the related timescale [133]. This tool will be mainly used to identify the reactions mostly related to the system's fast explosive timescale ($\tau_{e,f}$), i.e., the system's characteristic timescale, which controls the ignition delay time [121, 134–139]. It is noted that the system's characteristic mode must meet the following two conditions: (i) it has to be the fastest of the slow timescales, thus ensuring that the timeframe of action of that mode will be relevant to the system's slow evolution and (ii) its amplitude must be among the largest [133]. These conditions are met for the system's $\tau_{e,f}$ for all cases in the current study. Finally, it is worth noting that TPI reflects the relative importance of each reaction, since it is a quantity scaled against the sum of the absolute values of all TPIs for each mode. The TPI takes values from zero to +1 or -1 and the sum of the absolute values of all TPIs for each mode sum up to 1.

- the amplitude participation index (API), which measures the relative importance of each reaction to each CSP mode's amplitude (f^i) [140–142]. For the fast (exhausted) modes where by definition $f^i \approx 0$ due to the negligible projection of the vector field to the fast directions in the phase space, API identifies the reactions participating the most to the established equilibria [143, 144]. This tool has also been used for the characterisation of the flame topology, by accounting for the competition between transport and chemistry in the amplitudes of the slow (non-exhausted) modes [145–149]. For the slow modes, a positive API indicates a reaction which tends to increase the amplitude of the related mode, while the opposite applies for the negative API values. Like the TPI, the API takes values from zero to +1 or -1 and the sum of the absolute values of all APIs for each mode sum up to 1.

- the CSP Pointer (CSP Po), which identifies the variables (species mass fractions or temperature) mostly related to each CSP mode [122, 150]. This tool has been used for: (i) the development of reduced chemical kinetics models by identifying the variables mostly related to exhausted modes [151–153] and (ii) the introduction of an algorithmic method of ignition control, by identifying the variables mostly related to the system's characteristic CSP mode [105, 119, 154–156]. It is noted that by definition, the sum of all CSP Po values for each mode is equal to unity.

- the slow importance index (I^j_{slow}), which measures the relative importance of each reaction to the production (when positive) or consumption (when negative) of chemical species j (or to the increase/decrease of temperature). The slow importance index (I^j_{slow}) takes values from zero to +1 or -1 and the sum of the absolute values of all slow importance indices for each variable (species or temperature) sum up to 1. This tool has been used for: (i) the development of simplified (skeletal) chemical kinetics mechanisms [157–159] (ii) the characterization of ignition phenomena [160–162] and the (iii) determination of the importance of chemical/transport processes

for both major species and radicals [163, 164]. In the current work it will be used to identify the important reactions related to NO and N_2O. It is noted that the importance index is a scaled quantity, therefore, for the purpose of the current work, the unscaled importance index will also be used, denoted by $I^j_{slow,unsc}$.

All simulations were performed using the Chemkin-Pro program [165], while for the CSP analysis the CSPTk package [166] integrated with the TChem package [167] for thermo-kinetic database management was employed. For the determination of the number of fast modes, the criterion proposed in [168] was employed, along with absolute and relative tolerances of 10^{-8} and 10^{-2}, respectively.

3. Chemical dynamics

The analysis is split into two parts: the addition of H_2O_2 and the addition of H_2O. In the first part, the hydrogen-to-air ratio is kept constant and H_2O_2 is gradually added to the mixture, while in the second part, the fuel-to-air ratio is kept constant (with the fuel being 90%H_2-10%H_2O_2) and the mixture is gradually diluted with H_2O. Through this process, the results are quantified in detail, thus, enabling the determination of trends. In each part, the chemical dynamics is primarily explored at T(0)=900 K, in two aspects, namely the ignition delay time and NOx emissions. The investigation regarding NOx emissions is focused on NO and N_2O; the first is selected because it is the dominant contributor to NOx emissions (as it will also be demonstrated next) while the latter is the third most important greenhouse gas (after carbon dioxide and methane), thus, significantly contributing to global warming [169]. At the end of each sub-part the conclusions are extended to a range of initial temperatures. Although in all presented cases the pressure is kept fixed at 40 atm, the findings are relevant for a range of pressures ($\pm$ 10 atm) related to the operation of CI engines.

3.1. H_2O_2 addition

The hydrogen peroxide (H_2O_2) addition to the hydrogen/air mixture is performed at p(0)=40 atm and $\phi = 0.4$ in the context of homogeneous adiabatic constant pressure batch reactor simulations. The main analysis is performed for mixtures at T(0)=900 K but the results are extended to T(0)=800 and 1,000 K. These conditions aim to simulate the environment in a compression ignition engine cylinder at the top dead center. The hydrogen peroxide addition ranges from 0% (100% hydrogen) up to 15% (85% hydrogen) in fuel mole fraction. In order to properly assess the effect of the H_2O_2 addition, the hydrogen-to-air mole fraction ratio was kept constant (as in the pure hydrogen/air case at $\phi = 0.4$), and H_2O_2 was added on the basis of hydrogen's initial mole fraction. Conceptually, through this method, the hydrogen and air moles added to the combustion chamber are kept constant, while H_2O_2 is gradually added to the mixture. For clarity, Table 2 includes the initial compositions at the cases analysed in detail next.

Table 2: The initial mole fractions for the cases analysed in detail regarding the H_2O_2 addition.

% H_2O_2	$X_{H_2O_2}$	X_{H_2}	X_{O_2}	X_{N_2}	$X_{H_2}/(X_{O_2} + X_{N_2})$
0	0.000000	0.143836	0.179795	0.676370	0.168
1	0.001436	0.143629	0.179536	0.675398	0.168
5	0.007140	0.142809	0.178511	0.671540	0.168
10	0.014180	0.141796	0.177245	0.666779	0.168

3.1.1. Ignition delay time

The addition of H_2O_2 in fuel/air mixtures is a well-documented method of effective ignition promotion [104, 106, 117, 170], but its efficiency has never been tested in hydrogen combustion. Figure 1 shows that a mere 1% of H_2O_2 addition can incur a decrease in the ignition delay time by a factor of 5. With addition of 5% to 10% H_2O_2 the ignition delay time drops to 1-2 ms, which are typical ignition delay times for CI engines. In fact, Fig. 1 shows that the decrease in

the ignition delay time increases linearly to the H_2O_2 addition, roughly by a factor of 5, regardless the mixture's initial temperature. However, such huge acceleration of the ignition delay time is not accompanied by an increase in the equilibrium temperature which barely increases by 0.8% with 10% of H_2O_2 addition.

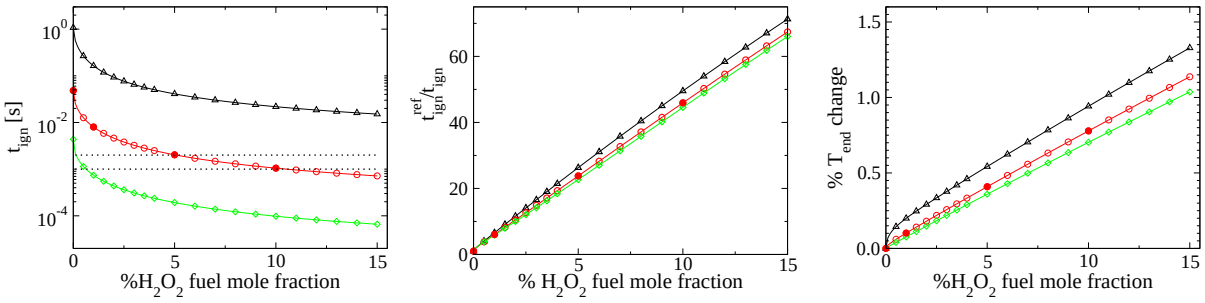

Figure 1: The effect of H_2O_2 addition during the homogeneous adiabatic constant pressure autoignition of a hydrogen/air mixture at p(0)=40 atm, $\phi = 0.4$ (triangles-T(0)=800 K, circles-T(0)=900 K, diamonds-T(0)=1,000 K), on the ignition delay time (left and middle) and the end (equilibrium) temperature (right). The blocked symbols represent the cases analysed in detail next. The dotted lines are placed at t_{ign}=1 and 2 ms.

The significant acceleration of the ignition process reflected on the ignition delay time decrease in Fig. 1 suggests an increase on the chemical radicals, which is indeed verified in Fig. 2. The H and OH mass fractions increase remarkably even with as little as 1% of H_2O_2 addition, thus highlighting the increased reactivity induced by the H_2O_2 addition. Moreover, Fig. 2 indicates that the increased reactivity affects the temperature evolution from the early stage of the ignition process, leading to an insignificant temperature increase.

From a dynamics perspective, the quantity that is correlated with the system's ignition delay time, is the system's characteristic timescale [142, 156], which for the cases under current study, this is $\tau_{e,f}$. Therefore, the system's characteristic timescale can be considered as a measure of the system's reactivity, thus, the faster the characteristic timescale, the more reactive the system. Figure 3 shows in pure hydrogen case, $\tau_{e,f}$ initially decelerates, then for the most part of the process remains roughly constant and at the final stage

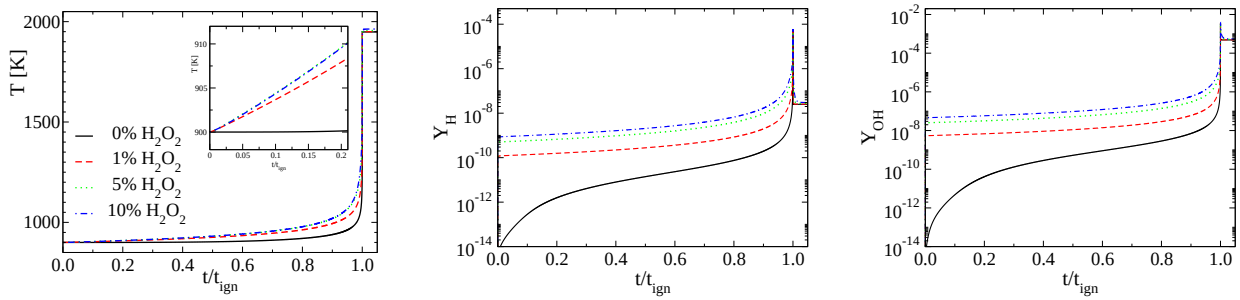

(a) (b) (c)

Figure 2: The evolution of temperature (a) and the mass fractions of H (b) and OH (c) as a function of time, scaled against the respective ignition delay times for the various cases of H_2O_2 initial fuel mole fraction, during the homogeneous adiabatic constant pressure autoignition of a hydrogen/air mixture at p(0)=40 atm, T(0)=900 K, $\phi = 0.4$.

of the process it rapidly accelerates and then decelerates, meets a slow explosive timescale ($\tau_{e,s}$) and then they both disappear. The disappearance of $\tau_{e,f}$ (and $\tau_{e,s}$) occurs very close to the point where the system reaches the maximum temperature rate of change, which in the current study it is used to measure the ignition delay time. It is noted that in Fig. 3 $\tau_{e,s}$ has been omitted in order to avoid any confusion with $\tau_{e,f}$, but it suffices to mention that $\tau_{e,s}$ is order of magnitudes larger than $\tau_{e,f}$ for the most part of the ignition process. Figure 3 shows that with the addition of H_2O_2, $\tau_{e,f}$ becomes generally faster, as this is indicated by the smaller values $\tau_{e,f}$ reaches for the most part of the process. In fact, Fig. 3 shows that the addition of H_2O_2 induces faster $\tau_{e,f}$ from the very beginning of the ignition process. Also, the H_2O_2 addition tends to decrease the deceleration $\tau_{e,f}$ experiences at the early part of the process and with 10% H_2O_2 this deceleration is roughly eliminated. As expected, in all cases, $\tau_{e,f}$ reaches the lowest value very close to the ignition delay time ($t/t_{ign} \approx 1$). However, the lowest $\tau_{e,f}$ value is roughly the same for all cases. This is a well documented finding that relates to the fact that in this region the dominant chemistry and its contribution to $\tau_{e,f}$ remain roughly the same [105, 144, 150, 156].

In order to understand the change in the physics that drives the ignition process due to the addition of H_2O_2, the TPIs of all reactions related to $\tau_{e,f}$ were

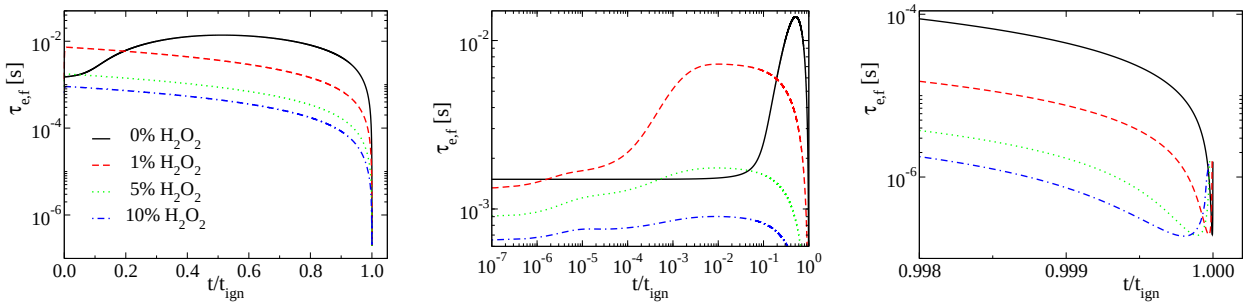

Figure 3: The temporal evolution of the system's fast explosive timescale $\tau_{e,f}$ as a function of time, scaled against the respective ignition delay times, for the various cases of H_2O_2's initial concentration, during the homogeneous adiabatic constant pressure autoignition of a hydrogen/air mixture at p(0)=40 atm, T(0)=900 K, $\phi = 0.4$.

calculated. Reactions with large associated TPI values have strong influence on the ignition delay time: positive TPI values indicate reactions that tend to decrease the ignition delay time while the opposite stands for the reactions associated with negative TPI values.

In the very early part of the ignition process Fig. 4 shows that reaction 9f is an important contributor to $\tau_{e,f}$ in all examined cases, with positive TPI values, favoring the explosive nature of $\tau_{e,f}$, thus promoting ignition. Although not explicitly shown in Fig. 4, reaction 9f is the main reason that the cases of added H_2O_2 all start with faster $\tau_{e,f}$ at $t = 0$ s. In fact, the relative contribution of 9f to $\tau_{e,f}$ increases with the addition of H_2O_2, (since the TPI of 9f increases). The increased role of 9f to the system's dynamics, after the addition of H_2O_2, is reasonable since 9f is a chain branching reaction that describes the dissociation of H_2O_2 to two OH radicals.

Figure 4 highlights two additional important differences between the pure hydrogen and H_2O_2 added cases. The first one relates to the decreasing relative contribution of 11b and the latter to the decreasing influence of 19/20f. Both reactions use HO_2 to produce H_2O_2. However, 11b accomplishes this using H_2 as a reactant and leads to the production of H radical, so it is essentially a chain branching, while the 19/20f requires another HO_2 mole and leads to the production of O_2. This explains why 11b has positive TPI and promotes ignition

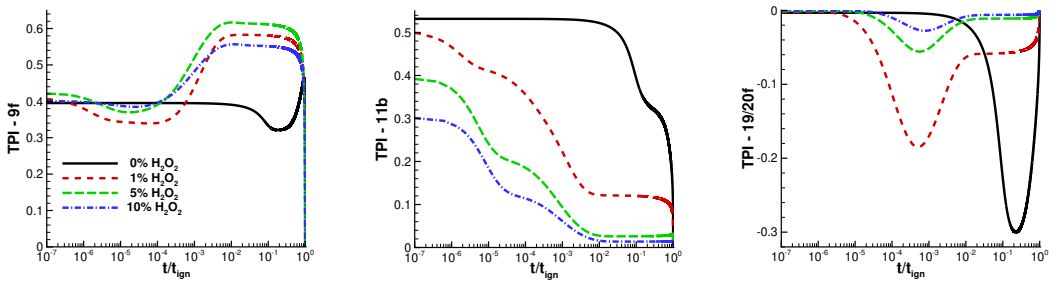

(a) (b) (c)

Figure 4: The largest TPIs, for the system's fast explosive timescale $\tau_{e,f}$ as a function of time, scaled against the respective ignition delay times, for the various cases of H_2O_2 addition, during the early part of the homogeneous adiabatic constant pressure autoignition process of a hydrogen/air mixture at p(0)=40 atm, T(0)=900 K, $\phi = 0.4$.

while 19/20f has negative TPI and opposes ignition; they are basically competing pathways, but the first is chain carrying that uses the fuel as reactant (which is abundant at this stage of the process), while the latter is a chain termination. With the addition of H_2O_2 in the initial composition, the requirement for H_2O_2 drops, which explains the decreasing relative effect of these two reactions, in a much more rapid manner compared to the pure hydrogen case.

For the largest part of the ignition process (in all cases) reaction 9f remains a major contributor to $\tau_{e,f}$ favoring its explosive character. However, as already explained the influence of 9f increases with the addition of H_2O_2. This is clearly shown in Fig. 5 which includes the reactions with the largest TPI values. In fact, the set of important reactions remains the same as in the very beginning of the process, i.e., reactions 9f, 11b and 19/20f, with one exception: the contribution of reaction 3f to $\tau_{e,f}$ increases significantly with the addition of H_2O_2. Reaction 3f is a chain branching reaction and uses OH radicals and the main fuel, i.e., H_2, to produce H_2O and H radicals. Since the production of OH radicals is strongly favored by 9f with the addition of H_2O_2 as previously explained, it is reasonable that the contribution of 3f increases when H_2O_2 is added to the mixture. It is noted that 3f is an exothermic reaction and the second largest contributor to the temperature rate of change; thus, its enhanced role contributes to the

increased temperature that is reached by the system throughout the process with the addition of H_2O_2.

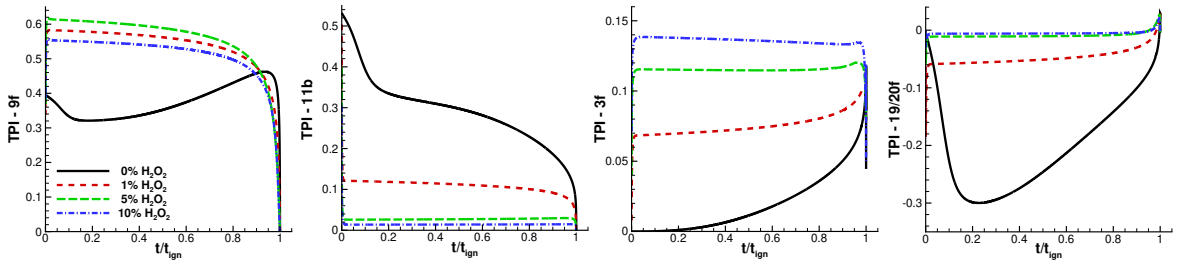

(a) (b) (c) (d)

Figure 5: The largest TPIs for the system's fast explosive timescale $\tau_{e,f}$ as a function of time, scaled against the respective ignition delay times, for the various cases of H_2O_2's initial concentration, during the main part of the homogeneous adiabatic constant pressure autoignition process of a hydrogen/air mixture at p(0)=40 atm, T(0)=900 K, $\phi = 0.4$.

At the late part of the ignition process, Fig. 6 shows that the dominant chemistry becomes roughly the same among the cases under study. In particular, reactions 5f and 21f become the main contributors to $\tau_{e,f}$, which explains the observation from Fig. 3 that at this part of the process, all cases obtain roughly the same minimum $\tau_{e,f}$ value. It is noted that reactions 5f and 21f are competing pathways, the first favors the explosive character of $\tau_{e,f}$ (as it is a chain branching reaction), while the latter favors the dissipative character of $\tau_{e,f}$ and tends to decelerate ignition. The importance of these two reactions at the late ignition stage is well documented in the litarture, thus, no further discussion on these is deemed necessary.

The system's chemical dynamics is investigated further in view of the CSP Po tool in order to identify the variables mostly related to the system's fast explosive mode. Figure 7 shows that H_2O_2 induces a dramatic change to the variables mostly associated with the fast explosive mode. In particular, in the pure hydrogen case, at the early stage of the ignition process, the mass fraction of HO_2 is the most important variable, followed by the mass fraction of H_2O_2. As the process evolves, the effect of HO_2 drops and that of H_2O_2 increases and

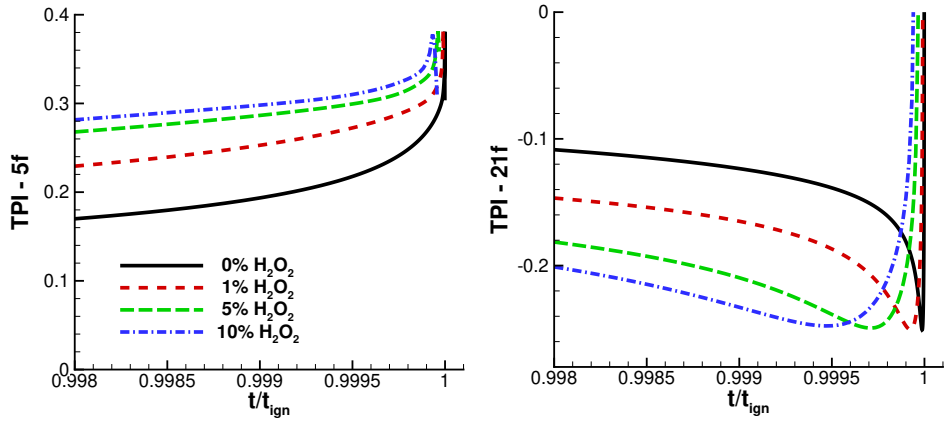

(a) (b)

Figure 6: The largest TPIs for the system's fast explosive timescale $\tau_{e,f}$ as a function of time, scaled against the respective ignition delay times, for the various cases of H_2O_2's initial concentration, during the late part of the homogeneous adiabatic constant pressure autoignition process of a hydrogen/air mixture at p(0)=40 atm, T(0)=900 K, $\phi = 0.4$.

becomes dominant and it is only at the late stage of the ignition process, temperature becomes dominant. However, with the addition of H_2O_2, temperature becomes the variable mostly associated with $\tau_{e,f}$ from the very early stage of the ignition process and remains as such until the end. Temperature's high CSP Po value concretely indicates the strong dependance of the system's evolution on temperature which is significantly enhanced by the addition of H_2O_2.

In order to extend the validity of the drawn conclusions to a range of initial temperatures, the same analysis was performed at T(0)=800 K and 1,000 K. The key findings were found to hold for all these examined conditions and this is briefly illustrated in the Supplementary material. The $\tau_{e,f}$ does not show any deceleration at the early part of the ignition process with 10%H_2O_2 at T(0)=800 and 1,000 K, similarly to what was reported for the T(0)=900 K case. Reaction 9f remains the dominant contributor to $\tau_{e,f}$ for the largest part of the ignition process, although its relative contribution decreases with increasing the initial temperature. Finally, temperature is the variable mostly related to the system's fast explosive mode, with minimal effect of system's initial temperature.

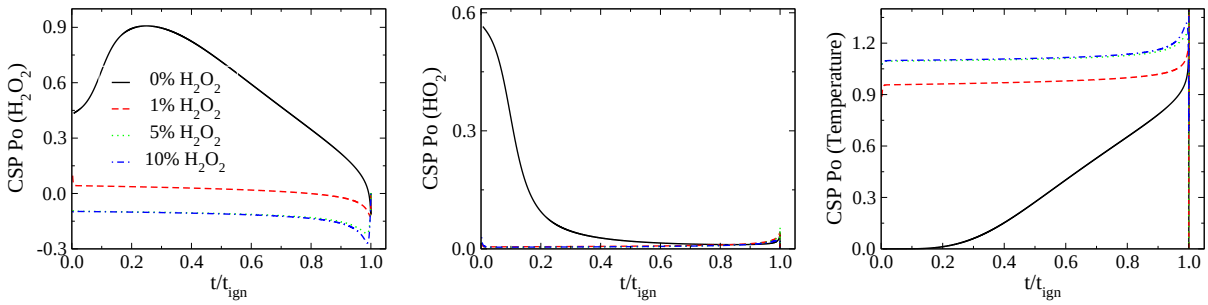

Figure 7: The largest CSP Po for the system's fast explosive timescale $\tau_{e,f}$ as a function of time, scaled against the respective ignition delay times, for the various cases of H_2O_2's initial concentration, during the homogeneous adiabatic constant pressure autoignition of a hydrogen/air mixture at p(0)=40 atm, T(0)=900 K, $\phi = 0.4$.

In summary:

- the decrease of the ignition delay time increases linearly with the addition of H_2O_2 by a factor of five due to the increase of the radical pool.
- the system's fast explosive timescale $\tau_{e,f}$ becomes faster with the addition of H_2O_2 from the beginning of the process.
- the system's increased ignitability through the addition of H_2O_2 is attributed to the enhanced effect of reactions 3f, 5f and 9f.

3.1.2. NOx formation

In this subsection, the effect of H_2O_2 addition on NOx production is investigated in detail, in view of NO and N_2O. This part of the study is significant for two reasons. Firstly, because to the best of the author's knowledge, such an investigation has not been reported in the literature and secondly, the results reported in the literature regarding the effect of H_2O_2 addition to carbon-based fuels on NOx production, are mixed. As already explained, H_2O_2 can be added to the fuel as a pure substance or as an additive to emulsified fuel. When added as a pure substance, H_2O_2 was reported to increase NO production in n-decane/air mixtures [100], methane/air mixtures [101, 171], ethanol/air mixtures [118] and

iso-octane/air mixtures [115], in HCCI mode operation [101, 115, 118], premixed laminar flames [171] and PSR mode [100]. On the other hand, as an additive to emulsified fuel, H_2O_2 was reported to reduce NOx with diesel [106–109, 111, 116, 120] and methane [104].

In the current work, H_2O_2 is added to the hydrogen/air mixture as a pure substance and as Fig. 8 reveals, there is a notable decreasing trend in the equilibrium values of NO and a small increasing trend of N_2O. In fact the decrease in NO is so strong that a 5% H_2O_2 addition can induce a ∼100% decrease in NO and <3% increase in N_2O. However, the percentage change of NO in equilibrium relative to the pure hydrogen case levels off after ∼ 5% H_2O_2, as opposed to N_2O which exhibits a linear increase. The decrease of NO and the increase of N_2O as a result of the H_2O_2 addition is insensitive to the mixture's initial temperature in the range of 800 K<T(0)<1,000 K. Finally, Fig. 8 confirms that the NO_2 production is indeed insignificant compared to NO, although there is a decreasing trend of the Y_{NO}/Y_{NO_2} ratio with decreasing the initial temperature.

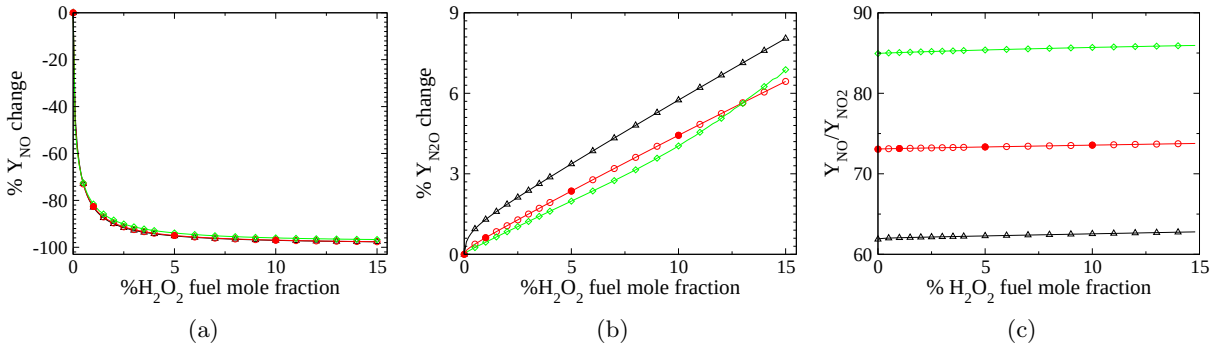

Figure 8: The effect of H_2O_2 addition in the homogeneous adiabatic constant pressure autoignition of a hydrogen/air mixture at p(0)=40 atm, $\phi = 0.4$ (triangles-T(0)=800 K, circles-T(0)=900 K, diamonds-T(0)=1,000 K), on the equilibrium mass fraction values of NO (a), N_2O (b) and NO_2 (c). The blocked symbols represent the cases analysed in detail next. All the equilibrium values displayed in the current figure were obtained at $t = 2 \times t_{ign}$.

Following the same practice as in Refs. [139, 144], the analysis of the NOx production will focus on the post-ignition region, as this is the part of the

process where NOx increase. Figure 9 displays the temporal evolution of the mass fractions of NO and H along with temperature. At first sight, it becomes evident that the mass fraction of NO and temperature, both increase rapidly in the post ignition region in the pure hydrogen case, as opposed to the cases with H_2O_2 addition which exhibit a more mild increase. The temperature's profile in this part of the process, will be discussed more next, because it is a finding of great significance. On the other hand, the mass fraction of H decreases rapidly in the pure hydrogen case, unlike the H_2O_2 added cases where H is depleted in a more moderate way. In fact, the gradients of NO, H and temperature decrease with the addition of H_2O_2.

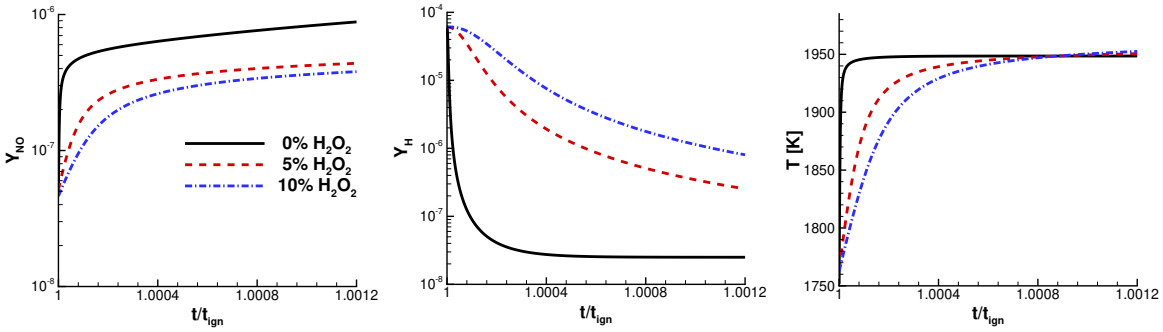

(a) (b) (c)

Figure 9: The temporal evolution of Y_{NO} (a), Y_H (b) and temperature (c), for the various cases of H_2O_2 addition, during the homogeneous adiabatic constant pressure autoignition of a hydrogen/air mixture at p(0)=40 atm, T(0)=900 K, $\phi = 0.4$.

In order to identify the chemical pathways that control the evolution of NO and N_2O, the slow importance index of the CSP theory is used. Starting with NO, Fig. 10 displays the reactions with the largest slow importance indices for the pure hydrogen case. It becomes evident that the mass fraction of NO is controlled by 2 main mechanisms: the thermal (Zeldovich) mechanism [172] and the NNH mechanism [173]. The former is a well established mechanism, while the latter is controversial [124]. For a detailed discussion about the origin of this controversy the reader is referred to the review work of [124]. Very briefly, the rate constant of 68f (which is a key reaction in the NNH mechanism) has

so far been determined with indirect experiments which suggest a value close to collision frequency, but these values contradict previous theoretical studies which indicate a much lower rate constant. Figure 10 shows that, in the early post-ignition part where NO exhibits a steep increase, the production of NO is mainly controlled by reactions 68f, 64f, 64b and 70f, the first two favoring its increase while the last two tend to deplete it. All these reactions relate to the NNH mechanism of NO production. Later in the post ignition part, reaction 63b becomes dominant, which is the most important reaction in the thermal NO mechanism. Reactions 3f/b and 7f/b, which are hydrogen related, play secondary (but not insignificant) roles, but shortly afterwards they reach an equilibrium state. Finally, reaction 151f plays a notable role, favoring the production of NO. Reaction 151f, is a well established mechanism of NO production [174] and it is known that its contribution to the NO production is of less significance, especially when compared to the thermal NO mechanism [124].

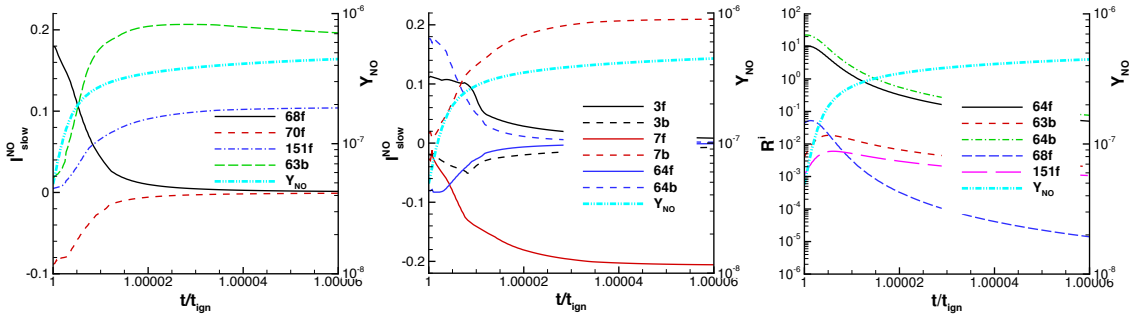

Figure 10: The largest slow Importance Indices for NO (I^{NO}_{slow}) and selected reaction rates (moles/(cm^{3}s)) in the pure hydrogen case, during the homogeneous adiabatic constant pressure autoignition of a hydrogen/air mixture at p(0)=40 atm, $\phi = 0.4$, T(0)=900 K.

The description of Fig. 10 regarding the key pathways that control NO production in the pure hydrogen case, can be summarised in Fig. 11. Concretely, NO is produced via the formation of NNH (reactions 64b and 68f, i.e., the NNH mechanism) and directly with oxygen atom reaction with nitrogen (reaction 63b, thermal NO mechanism), the first being dominant early in the post ignition part

while the second dominates later. Obviously, the reactions that compete the formation of NO in the NNH mechanism, i.e., reactions 64f and 70f, have negative importance indices, and they tend to decrease the formation of NO. The aforementioned mechanisms are coupled with hydrogen-related reactions (3f/b and 7f/b), which produce or consume the important O and H radicals.

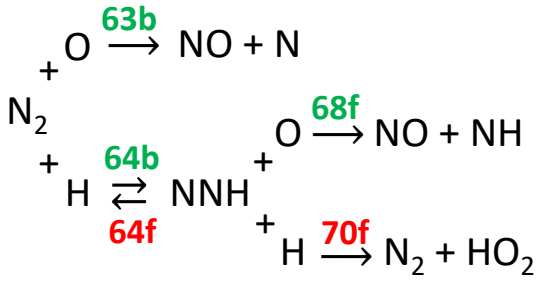

Figure 11: The main chemical pathway that controls the production of NO, in the post-ignition region, during the homogeneous adiabatic constant pressure autoignition of a hydrogen/air mixture (no additive) at p(0)=40 atm, $\phi = 0.4$, T(0)=900 K. Reactions in green have positive importance index, thus, favor the increase of NO, while reactions in red have negative importance index, therefore, tend to decrease NO.

Before moving to the discussion of the CSP diagnostics for the cases with the addition of H_2O_2, the profile of temperature in the part around the ignition delay time is discussed. As it was shown in Fig. 9, H_2O_2 addition leads to a decrease of temperature early in the post-ignition part. This is counterintuitive considering that, as it was shown in Fig. 2, temperature increases faster with the addition of H_2O_2 from the very beginning of the ignition process. Figure 12 displays the temperature evolution for the pure hydrogen and the 10%H_2O_2 cases, in the neighbourhood of the ignition delay time. As it is shown, the addition of H_2O_2 induces a significantly less steep increase of temperature. A budget analysis for the contribution of each reaction to the temperature equation was performed, following the same practice as in Ref. [133], which highlighted that the two most important contributors to the temperature rate of change are reactions 5f and 21f, the former being endothermic, thus tends to decrease temperature, while the latter being exothermic, thus, enhancing temperature increase. These two

reactions are competing each other, as they include the same reactants, the only exception being that 21f is a third body reaction. Obviously, the contribution of 21f is much higher than 5f, since it drives the temperature increase. With the addition of H_2O_2, both reactions are favored, but in a disproportional manner, i.e., reaction 5f is favored more than 21f. As a result, reaction 5f acts as a "thermal scavenger" in this region and limits the temperature increase. This is illustrated more clearly in Fig. 12, where the ratio of the contributions of 5f and 21f to the temperature rate of change, has been plotted for the pure hydrogen and the 10% H_2O_2 cases; the ratio is very well correlated to the temperature evolution in both cases. Temperature's mild increase with the addition of H_2O_2 will be the key element for the significant impact of the production of NO, as it will be shown next.

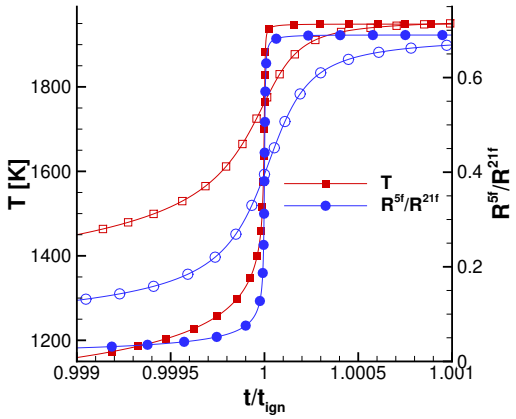

Figure 12: The evolution of temperature and the ratio of the absolute values of the terms related to reactions R^{5f} and R^{21f} in the temperature equation, during the homogeneous adiabatic constant pressure autoignition of hydrogen/air and 90%hydrogen-10%H_2O_2/air mixture (blocked and hollow symbols, respectively) at p(0)=40 atm, $\phi = 0.4$, T(0)=900 K.

In fact, the addition of H_2O_2 does not affect the set of most important reactions for the production of NO. Figure 13 shows that the two mechanisms previously described, i.e., the thermal and the NNH mechanisms, remain the main pathways for NO production after the addition of H_2O_2. However, signifi-

cant quantitative differences do exist. Firstly, the contributions of the reactions related to the NNH mechanism (reactions 64f, 64b, 68f, 70f), drop in magnitude and the timeframe they are active, is shifted later to the post-ignition area and extended. Secondly, the contribution of reaction 63b (part of the thermal NO mechanism) also drops in magnitude in the early post-ignition part, where NO experiences the steep increase. Therefore, in overall, it can be concluded that both the thermal and the NNH mechanisms remain the key mechanisms of NO production after the addition of H_2O_2, but their contributions decrease in magnitude due to the decreased temperature in the early post-ignition part.

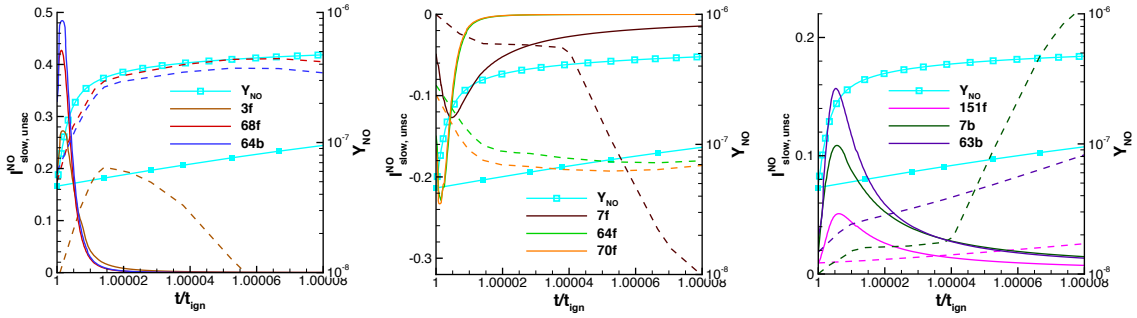

(a) (b) (c)

Figure 13: The largest unscaled slow importance indices for NO ($I^{NO}_{slow,unsc}$) for the 0% and 10% H_2O_2 addition cases (solid and dashed lines, respectively), overlaid with the mass fraction of NO (hollow and blocked square symbols for the 0% and 10% H_2O_2 addition cases, respectively), at p(0)=40 atm, $\phi = 0.4$, T(0)=900 K; both cases simulate homogeneous adiabatic constant pressure autoignition.

In order to extend the validity of the conclusions to a range of initial temperatures, the same analysis was repeated for the cases of T(0)=800 K and 1,000 K and quantitative evidence is provided in the Supplementary material. It was found that even at these conditions, the NNH mechanism remains the key mechanism for NO production in the early post-ignition area, while thermal NO becomes dominant shortly afterwards. An increasing trend of the importance and the rate of reaction 68f, with increasing the initial temperature was observed, which is related to the higher temperatures reached by the system.

The second NOx emission pollutant discussed in the current study, is the

N_2O. As it was shown in Fig. 8, unlike NO, N_2O increases monotonically with the addition of H_2O_2. This is also shown in Fig. 14 which compares the temporal evolution of N_2O in the early post-ignition part for the pure hydrogen case, along with the 5% and 10% of H_2O_2 addition. Atomic O is also shown to increase with the addition of H_2O_2. As it will be shown next, O atoms are essential for the creation of N_2O. Note, however, that as shown in Fig. 8, the increase induced on N_2O due to the addition of H_2O_2, is quite small, therefore, any differences in the chemical pathways are expected to be also small.

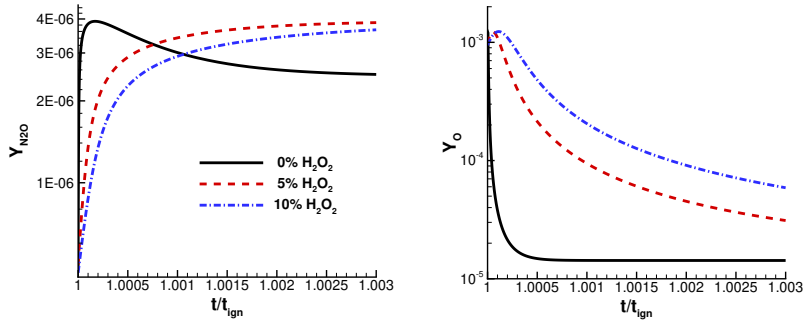

Figure 14: The temporal evolution of Y_{N_2O} (a) and Y_O (b), for the various cases of H_2O_2 addition, during the homogeneous adiabatic constant pressure autoignition of a hydrogen/air mixture at p(0)=40 atm, T(0)=900 K, $\phi = 0.4$.

In order to identify the changes in the chemical pathways related to N_2O production, the key pertinent chemistry in the no-additive (pure hydrogen) case has to be analysed. For this purpose, the largest slow importance indices for N_2O, in the pure hydrogen case were calculated and are displayed in Fig. 15. It is shown that N_2O production is mainly favored by reactions 7b and 149b; the first produces O radicals which are used in the second as reactants to react with N_2 and create N_2O. The reverse of these reactions, i.e., 7f and 149f, both also play key role and have insignificant indices. However, they both tend to decrease the N_2O production, which is reasonable since they compete the reverse pathway.

With the addition of H_2O_2, the main chemical pathway that controls the

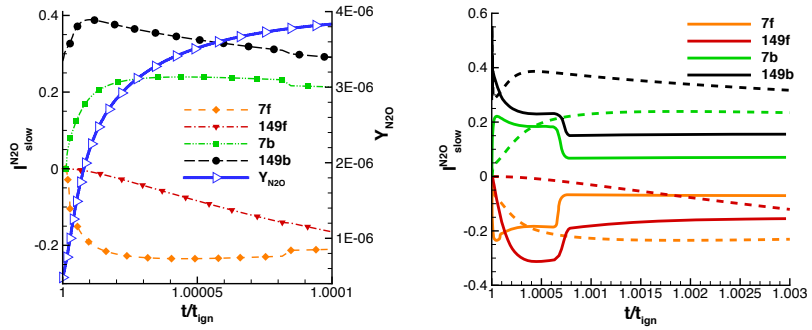

(a) (b)

Figure 15: (a) The largest slow importance indices for N_2O ($I_{slow}^{N_2O}$), overlaid with the mass fraction of NO, during the homogeneous adiabatic constant pressure autoignition of a hydrogen/air mixture (no additive) at p(0)=40 atm, $\phi = 0.4$, T(0)=900 K. (b) The largest slow Importance Indices for N_2O ($I_{slow}^{N_2O}$) for the 0% and 10% H_2O_2 addition cases (solid and dashed lines, respectively) to the hydrogen/air mixture at p(0)=40 atm, $\phi = 0.4$, T(0)=900 K; both cases refer to homogeneous adiabatic constant pressure autoignition.

N_2O production remains the same, as illustrated in Fig. 15. However, the importance of 149b increases whereas that of the reverse, i.e., 149f drops, resulting in an increased production of N_2O. The enhanced role of 149b, which requires O radicals, is mainly (but not exclusively) due to reaction 7b, which produces O radicals through the consumption of OH radicals. The increased relative importance of 7b can be attributed to the larger pool of OH radicals, achieved with the addition of H_2O_2. The increased role of 149b in the production of N_2O is further supported by the profile of the respective reaction rate, which increases significantly with the addition of H_2O_2 as opposed to the rate of R^{149f} which exhibits only small change. Quantitative evidence for this finding is provided in the Supplementary material.

The conclusions drawn for the H_2O_2 addition regarding the N_2O production at T(0)=900 K can be extended to a range of 800 K<T(0)<1,000 K, as demonstrated in the Figures included in the Supplementary material. In particular, the importance of reaction 149b remains high for both 800 K and 1,000 K at 10% H_2O_2 addition. In fact, the importance of 149b, in view of the importance

index and the reaction rate, increases monotonically with temperature, from 800 K up to 1,000 K.

In summary:

- the H_2O_2 has a strong effect on the mass fractions NO and NO_2, decreasing substantially their production, and a weak effect on N_2O, favoring its increase. Indicatively, a 5% addition of H_2O_2 leads to ∼100% decrease of NO and NO_2 and <3% increase of N_2O.

- with the addition of H_2O_2, the contributions of the competing reactions 5f and 21f to the temperature rate of change become enhanced but the former (which tends to decrease the temperature rate of change) is favored significantly more than the latter (which tends to increase the temperature rate of change), therefore, the temperature exhibits a milder increase in the neighborhood of the ignition delay time.

- the thermal and the NNH mechanisms remain the main pathways for the production of NO after the addition of H_2O_2, but their effects weaken due to the decreased temperature in the early post-ignition part.

- the increased production of N_2O after the addition of H_2O_2 is associated with the increased production of O radicals and is due to the increased role of reactions 149b and 7b.

3.2. H_2O addition

In this section, the effect of H_2O addition to the mixture is investigated. In order to properly assess the implications on the ignition delay time and NOx emissions, the H_2O_2 initial content is kept constant at 10% (fuel mole fraction) for all mixtures and cases investigated. Like in the previous section, the addition of H_2O will be performed gradually, and the 1-, 3- and 5-H_2O cases reflect the initial mole of H_2O as compared to H_2. In essence, the 1-, 3- and 5-H_2O cases represent the cases where the initial mole fraction of H_2O was ×1, ×3 and ×5 the mole fraction of the main fuel (hydrogen). Similar to the addition of H_2O_2,

in the cases of H_2O addition, the ratio of the mole fractions of hydrogen over air is kept fixed. For clarity, Table 3 includes the initial compositions of the cases analysed in detail next.

Table 3: The initial mole fractions for the cases of H_2O addition, analysed in detail.

H_2O case	$X_{H_2O_2}$	X_{H_2}	X_{O_2}	X_{N_2}	X_{H_2O}	$X_{H_2}/(X_{O_2} + X_{N_2})$	$X_{H_2O_2}/X_{H_2}$	X_{H_2O}/X_{H_2}
0-	0.014180	0.14180	0.17725	0.66678	0.00000	0.168	0.1	0
1-	0.012419	0.12419	0.15523	0.58397	0.12419	0.168	0.1	1
3-	0.0099479	0.099479	0.12435	0.46779	0.29844	0.168	0.1	3
5-	0.0082971	0.082971	0.10371	0.39016	0.41486	0.168	0.1	5

3.2.1. Ignition delay time

Starting the analysis with the effect on the ignition delay time, Fig. 16 displays the variation of the ignition delay time as a function of the initial quantity of H_2O. The addition of H_2O has moderate effect on the system's ignition delay time, but in any case it leads to its increase. This effect becomes more pronounced as the system's initial temperature increases. At T(0)=900 K, the addition of ∼0.4 mole fraction of H_2O (5-H_2O case) yields an ignition delay time less than 2 ms, which can be considered reasonable for compression ignition engine operation. The ignition delay increase induced by the addition of H_2O is accompanied by a significant decrease of the system's end (equilibrium) temperature, which in the 5-H_2O case it reaches roughly ∼25%. Unlike the effect on the ignition delay time which becomes more pronounced as the initial temperature increases, the effect on the end temperature decrease is insensitive to the system's initial temperature.

The analysis next will be performed on the basis of the following 4 cases, that will enable the identification of the trends in the changes of the key chemical pathways, induced by the addition of H_2O: 0-, 1-, 3-, 5-H_2O. Figure 17 displays the temporal evolution of temperature along with selected radicals for the four cases. Firstly, it is verified that the system's end temperature decreases with the addition of H_2O. However, it is counterintuitive that in the pre-ignition part of the process, temperature increases faster with the addition of H_2O. Also, the

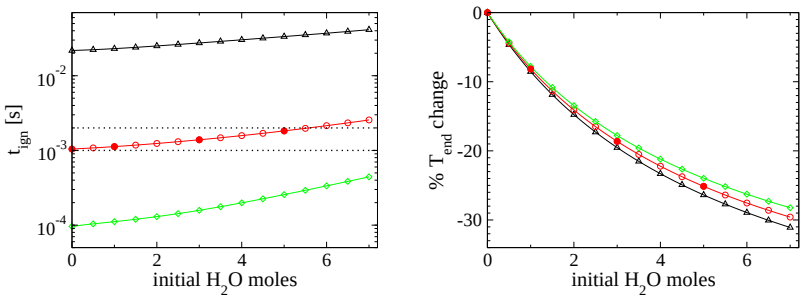

(a) (b)

Figure 16: The effect of H_2O addition during the homogeneous adiabatic constant pressure autoignition of a hydrogen/air mixture at p(0)=40 atm, $\phi = 0.4$ (triangles-T(0)=800 K, circles-T(0)=900 K, diamonds-T(0)=1,000 K), on the ignition delay time (a) and the end (equilibrium) temperature (b). The blocked symbols represent the cases analysed in detail next. The dotted lines are placed at t_{ign}=1 and 2 ms.

addition of H_2O at sufficiently high initial quantities such as in the 3- and 5-H_2O cases, results in the formation of a clear two-stage ignition process. It is noted that the 2-stage ignition depicted in the temperature graphs is also reflected to the respective heat release rate profiles (see relevant graphs in the Supplementary Material). All these findings will be discussed in more detail next. In addition, the OH and HO_2 radicals increase faster with the addition of H_2O, for the most part of the process; however, at the end of the ignition process and before the occurrence of the inflection point which marks the ignition delay time, their increase is not only halted but in fact for sufficiently high initial concentration of H_2O (e.g., the 3- and 5-H_2O cases), they exhibit a decrease. This counterintuitive behavior will also be discussed in more detail next, but at this point it becomes clear that it is related to the emergence of the second ignition stage.

The timescale that is the characteristic one and correlated with the ignition delay time in the cases under study is the fast explosive one, i.e., $\tau_{e,f}$. The evolution of $\tau_{e,f}$ for the four cases of H_2O addition is displayed in Fig. 18. Firstly, it can be seen that at the very beginning of the ignition process, $\tau_{e,f}$ is barely affected by the addition of H_2O. This is important because it is consistent with

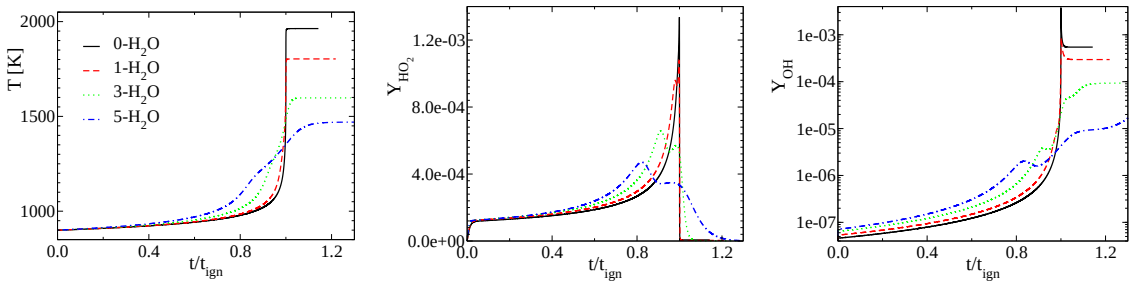

(a) (b) (c)

Figure 17: The temporal evolution of temperature (a), Y_{HO_2} (b) and Y_{OH} (c), as a function of time, scaled against the respective ignition delay times for the various H_2O addition cases, during the homogeneous adiabatic constant pressure autoignition of a 90%H_2-10%H_2O_2/air mixture at p(0)=40 atm, T(0)=900 K, $\phi = 0.4$.

the final outcome, i.e., the ignition delay time does not increase a lot with the addition of H_2O. In fact, for the most part of the ignition process, $\tau_{e,f}$ is largely insensitive to the addition of H_2O and accelerates moderately. However, at the end of the ignition process significant differences emerge, which become more pronounced as the H_2O addition increases. In particular, at sufficiently high H_2O addition (e.g., 3-H_2O and 5-H_2O), $\tau_{e,f}$ starts decelerating much earlier than $t/t_{ign} = 1$ and, in fact, there is no steep acceleration of $\tau_{e,f}$ close to the end of the ignition process, as occurs in the 0-H_2O case.

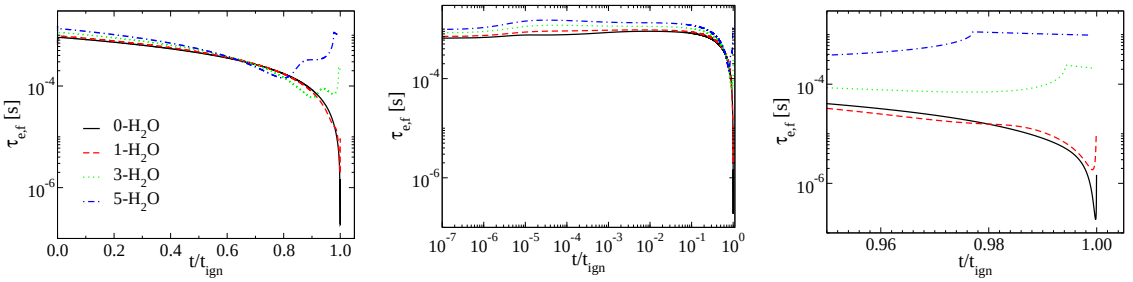

(a) (b) (c)

Figure 18: The evolution of the system's fast explosive timescale $\tau_{e,f}$ as a function of time, scaled against the respective ignition delay times, for the various H_2O addition cases, during the homogeneous adiabatic constant pressure autoignition of a 90%H_2-10%H_2O_2/air mixture at p(0)=40 atm, T(0)=900 K, $\phi = 0.4$.

In order to identify the reactions that mostly relate to $\tau_{e,f}$, thus having the largest effect on the ignition delay time control, for the H_2O addition cases, the

TPIs related to $\tau_{e,f}$ were calculated. In the early part of the ignition process where $\tau_{e,f}$ is barely affected by the addition of H_2O, the differences in the TPIs are fairly small, as shown in Fig. 19. Reaction 9f is the dominant one followed by the contribution of 11b which drops fairly fast. Both reaction 9f and 11b favor the explosive character of $\tau_{e,f}$, thus, promote ignition. Reactions 3f and 18f play secondary roles, the first favoring and the second opposing the explosive character of $\tau_{e,f}$. In terms of trends, the addition of H_2O: (i) boosts the role of 9f, as the ignition process progresses and remains the dominant contributor to $\tau_{e,f}$ for the most part of the process, (ii) promotes the role of 11b very briefly, in the very early part of the ignition process, (iii) favors the role of 3f more increasingly as the ignition process evolves and (iv) advances the role of 18f for a brief period of time in the early part of the ignition process. The advanced role of 9f as a result of the the addition of H_2O can be explained by the fact that it is a third body chain branching reaction leading to the formation of the highly reactive OH radical, and the efficiency of H_2O in that reaction is the second largest (with a value of 7.65) and only slightly smaller than that of H_2O_2 (with a value of 7.70). The advancing of that particular reaction due to the addition of H_2O has also been confirmed in the ignition of methane [144]. Reactions 3f and 18f which both exhibit higher TPIs due to the addition of H_2O, both include OH in the reactants, the first in combination with the main fuel (H_2) and the latter with HO_2.

During the main part of the ignition process, the reactions with the largest contributions to $\tau_{e,f}$ are reactions 9f, 3f and 13/14f, the first two favoring and the last one opposing the explosive character of $\tau_{e,f}$, as it is depicted in Fig. 20. All three increase their contributions with the addition of H_2O. The reason for the increased role of 9f and 3f was previously discussed while for reaction 13/14f, its contribution is slightly advanced because it includes OH radical in the reactants, a species that is promoted due to the increased role of 9f. During this part of the process, the radical pool increases and this increase is enhanced with the addition of H_2O, mainly due to the advanced roles of 9f and 3f.

The last part of the ignition process is probably the most interesting one,

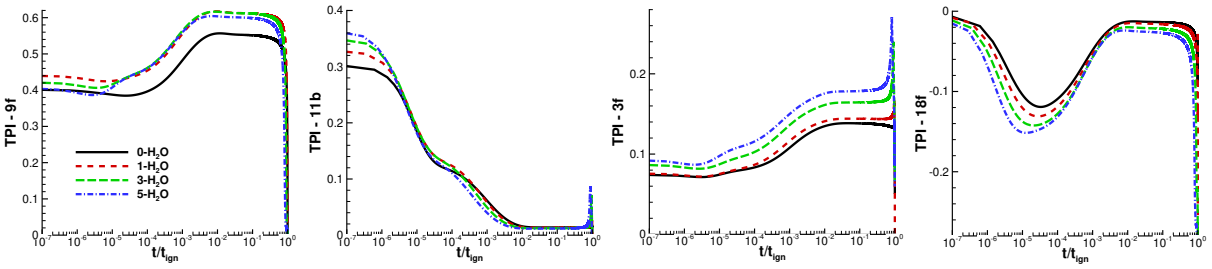

(a) (b) (c) (d)

Figure 19: The largest TPIs for the system's fast explosive timescale $\tau_{e,f}$ as a function of time, scaled against the respective ignition delay times, for the various H_2O addition cases, during the early part of the homogeneous adiabatic constant pressure autoignition of a 90%H_2-10%H_2O_2/air mixture at p(0)=40 atm, T(0)=900 K, $\phi = 0.4$.

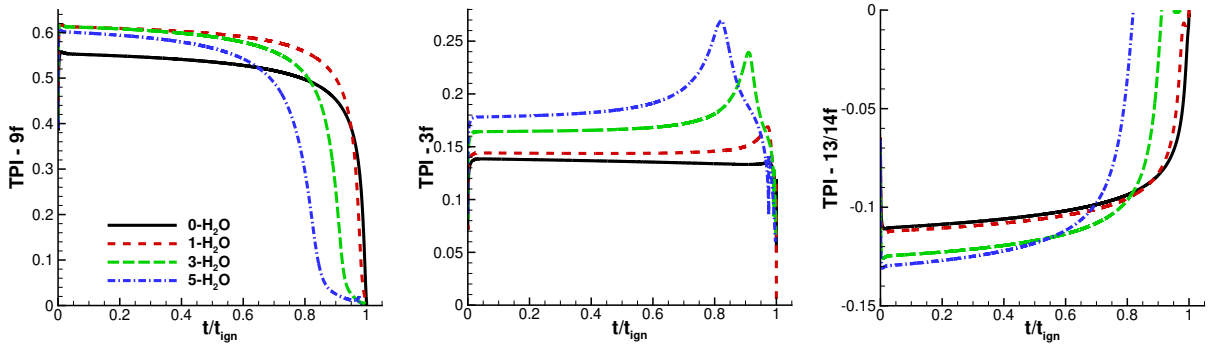

(a) (b) (c)

Figure 20: The largest TPIs for the system's fast explosive timescale $\tau_{e,f}$ as a function of time, scaled against the respective ignition delay times, for the various H_2O addition cases, during the main part of the homogeneous adiabatic constant pressure autoignition of a 90%H_2-10%H_2O_2/air mixture at p(0)=40 atm, T(0)=900 K, $\phi = 0.4$.

because it is at this part that for sufficiently high H_2O addition the system exhibits a second ignition stage. In the 0-H_2O case, the largest contributors to $\tau_{e,f}$ were identified (and confirmed in Fig. 21) to be reactions 5f and 21f, the former favoring and the latter opposing the explosive character of $\tau_{e,f}$. The relative contributions of these two reactions is diminished significantly as the H_2O addition increases. In fact, 21f becomes practically insignificant for sufficiently high H_2O added cases, such as the 3-H_2O and 5-H_2O cases. It is reminded that reaction 21f is a highly exothermic reaction and as it was shown in the previous section, it was the main contributor to the temperature increase in the late

ignition stage. While the contributions of 5f and 21f to $\tau_{e,f}$ decrease dramatically as H_2O is added, the contributions of 3f and most importantly that of 18f increase, the former favoring and the latter opposing the explosive character of $\tau_{e,f}$. All these findings suggest that the second ignition stage that emerges for sufficiently high H_2O added cases is due to primarily the boosted role of 18f and secondarily the decreased contribution of 5f. The combined effect from these two reactions results in the early deceleration of $\tau_{e,f}$ and the emergence of the second ignition stage. Reaction 18f is a chain termination reaction (leads to the formation of H_2O and O_2) which explains its tendency to oppose the explosive character of $\tau_{e,f}$ and decelerate ignition. There is probably not only one reason why this reaction is favored at this part of the process. Firstly, it includes OH as a reactant, which is a species that is particularly favored by the addition of H_2O, mainly through reaction 9f. The second reactant is the HO_2 radical which is also increased due to the addition of H_2O, as it was shown in Fig. 17. Moreover, it is the only reaction with a negative activation energy, therefore, its rate constant is already high when reaching the high temperature regime.

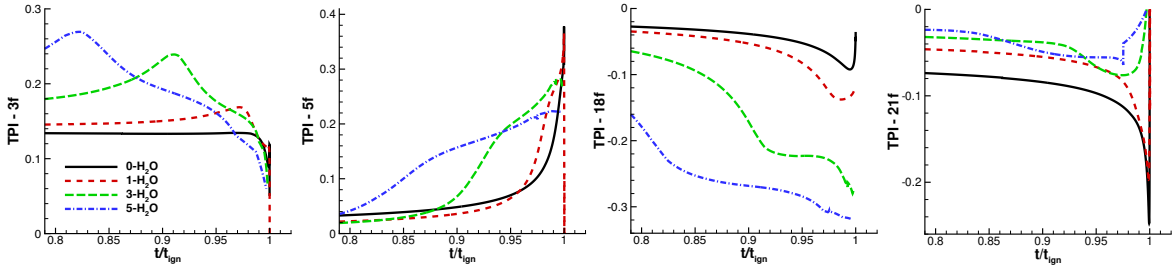

(a) (b) (c) (d)

Figure 21: The largest TPIs for the system's fast explosive timescale $\tau_{e,f}$ as a function of time, scaled against the respective ignition delay times, for the various H_2O addition cases, during the late part of the homogeneous adiabatic constant pressure autoignition of a 90%H_2-10%H_2O_2/air mixture at p(0)=40 atm, T(0)=900 K, $\phi = 0.4$.

In terms of the variables that are mostly related to the system's fast explosive mode, the CSP Po in Fig. 22 highlights the importance of temperature in all H_2O addition cases, which is reasonable considering that the role of reaction 9f remains significant. However, the relation of H_2O_2 to the fast explosive mode

is enhanced with the addition of H_2O, which can be explained by the enhanced roles of reactions 9f and 13/14f, where it is reactant. The key point here is that even after significant addition of H_2O, the system is still strongly controlled by temperature and mainly evolves in a thermal runaway.

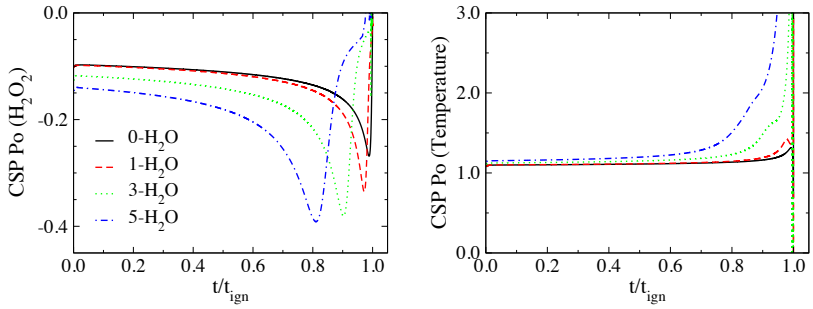

(a) (b)

Figure 22: The largest CSP Po for the system's fast explosive timescale $\tau_{e,f}$ as a function of time, scaled against the respective ignition delay times, for the various H_2O addition cases, during the homogeneous adiabatic constant pressure autoignition of a 90%H_2-10%H_2O_2/air mixture at p(0)=40 atm, T(0)=900 K, $\phi = 0.4$.

To extend the validity of the findings previously reported regarding the effect of H_2O addition on the ignition delay time, the analysis was repeated at T(0)=800 K and 1,000 K. Figure 23 reveals that the two stage ignition is enhanced for high initial temperatures and tend to diminish for lower ones. The two stage ignition is reflected on the system's $\tau_{e,f}$ which does not experience a steep acceleration close to the inflection point as it was reported in the 0-H_2O case. Reaction 18f plays a key role opposing the explosive character of $\tau_{e,f}$ and its role is enhanced as the initial temperature increases. This confirms further the correlation between the emergence of second ignition stage and reaction 18f. Finally, temperature remains the variable mostly related to the system's fast explosive mode regardless the initial temperature.

In summary:

- The addition of H_2O has moderate effect on the system's ignition delay time, favoring its increase.

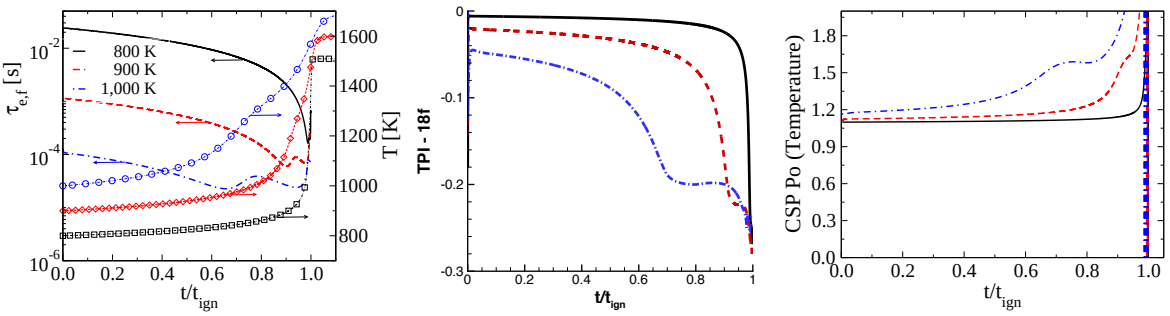

(a) (b) (c)

Figure 23: The system's fast explosive timescale $\tau_{e,f}$ (a), the TPI of reaction 18f related to the system's $\tau_{e,f}$ (b) and the CSP Po of temperature related to the system's $\tau_{e,f}$ (c), during the homogeneous adiabatic constant pressure autoignition of a 90%hydrogen-10%H_2O_2/air mixture, diluted by 30% with H_2O, at p(0)=40 atm, $\phi = 0.4$, for T(0)=800, 900 and 1,000 K.

- At conditions of sufficient steam dilution, the system ($H_2/H_2O_2/H_2O$/air) exhibits a two-stage ignition which is the result primarily of the increased role of reaction 18f and the decreased role of 21f, and secondarily of the decreased role of reaction 5f.

- The two-stage ignition of $H_2/H_2O_2/H_2O$/air mixtures is favored with the increase of the initial temperature.

3.2.2. NOx formation

In the previous subsection (Fig. 16) it was reported that the addition of H_2O induces a substantial decrease on the system's end (equilibrium) temperature. Therefore, it is expected that the production of NOx emissions, also drops significantly. This is indeed the case, as it is shown in Fig. 24. In fact, the decrease of NO and N_2O is so large that it can be properly assessed only if compared as a ratio against the respective undiluted (0-H_2O) case, rather than percentage change. For instance, in the 1- and 3-H_2O cases, NO decreases by two and four orders of magnitude, respectively, while the N_2O exhibits more moderate decrease (roughly a factor of two and seven, respectively). The spectacular decrease of NO is largely insensitive to the initial temperature for relatively small H_2O addition, but for high H_2O addition it does exhibit some moderate

dependance. On the other hand, the N_2O decrease is generally insensitive to the system's initial temperature.

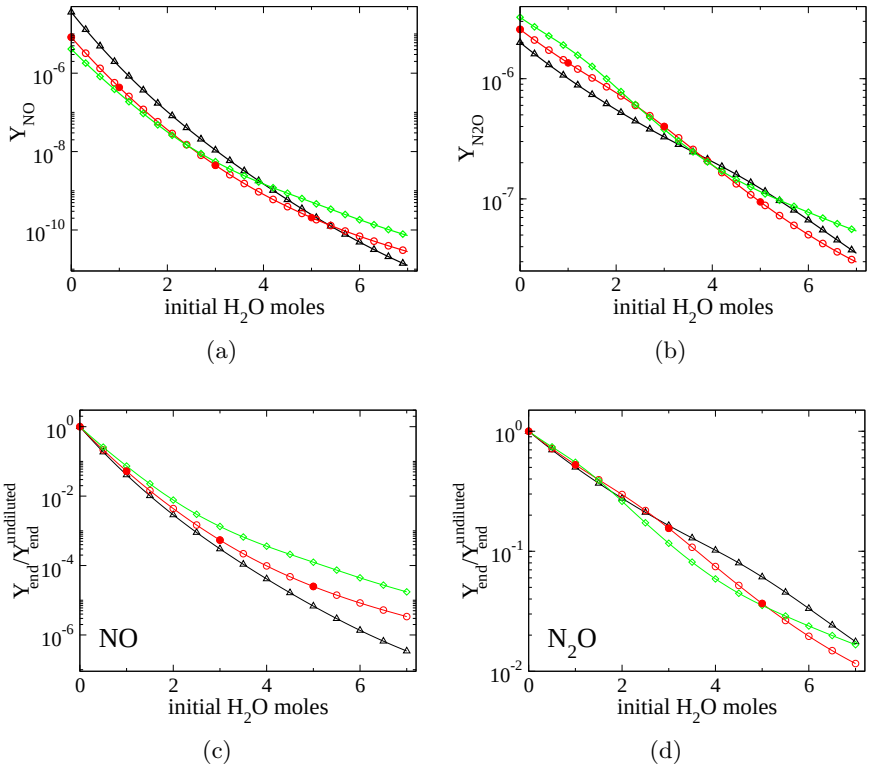

Figure 24: The effect of H_2O addition in the homogeneous adiabatic constant pressure autoignition of a 90%H_2-10%H_2O_2/air mixture at p(0)=40 atm, ϕ = 0.4 (triangles-T(0)=800 K, circles-T(0)=900 K, diamonds-T(0)=1,000 K), on the equilibrium mass fraction values of NO (a,c) and N_2O (b,d). The blocked symbols represent the cases analysed in detail next.

To understand the mechanism that affects the production of NO though the addition of H_2O, we focus on the post ignition part of the process. Figure 25 shows that the increase in NO due to H_2O addition, is accompanied by an increase in the remaining H_2, and significant decreases of H radicals and temperature. Note that the decrease in H radicals occurs early in the early part of the post-ignition area, while later this decrease is diminished.

In order to properly assess the changes in the chemical pathways pertinent

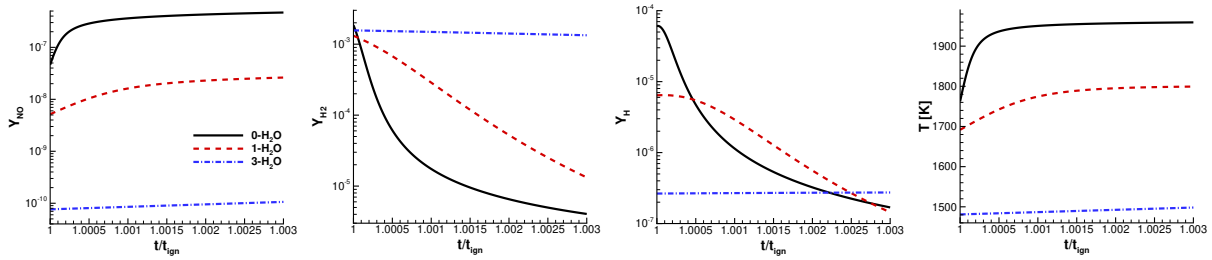

Figure 25: The temporal evolution of Y_{NO} (a), Y_{H_2} (b), Y_H (c) and temperature (d), for the various H_2O addition cases, during the homogeneous adiabatic constant pressure autoignition of a 90%H_2-10%H_2O_2/air mixture at p(0)=40 atm, T(0)=900 K, $\phi = 0.4$.

to NO, the unscaled have been used and plotted in Fig. 26. The set of chemical reactions that control the evolution of NO does not change with the addition of H_2O. The first observation that is clear is that reaction 3f experiences a decrease in the associated unscaled importance index, but its decrease is much smaller compared to the rest of the set, therefore, it becomes the largest contributor to the NO, favoring its production. Secondly, the NNH and thermal (Zeldovich) both remain the key mechanisms that drive the formation of NO (reactions 64b-68f-64f-70f and 63b, respectively), the former in the early post ignition part and the latter afterwards, however, their unscaled importance indices drop two orders of magnitude. Finally, reactions 151f, 7f and 7b remain notable contributors especially in the late post-ignition part, but their contributions drop, likewise, roughly two orders of magnitude. Considering that the decrease of the NO mass fraction in the 1-H_2O case is roughly two orders of magnitude (Fig. 25), it becomes perfectly reasonable that the unscaled indices of the most important reactions all drop roughly two orders of magnitude as well.

In view of the CSP modes, the examination of the CSP mode that is mostly related to NO (i.e., the CSP mode that the largest CSP pointer value is related to NO), reveals in Fig. 27 that the related amplitude drops and the associated timescale increases with the addition of H_2O. It is reminded that the timescale

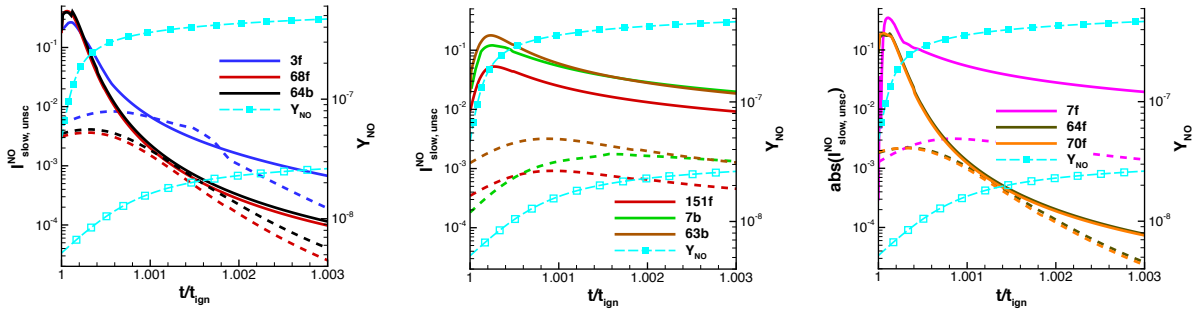

Figure 26: The largest unscaled slow importance indices for NO ($I^{NO}_{slow,unsc}$) for the 0% and 10% H_2O addition cases (solid and dashed lines, respectively), overlaid with the mass fraction of NO (hollow and blocked square symbols for the 0% and 10% H_2O addition cases, respectively), during the homogeneous adiabatic constant pressure autoignition of a 90%H_2-10%H_2O_2/air mixture at p(0)=40 atm, T(0)=900 K, ϕ = 0.4. The indices related to reactions 7f, 64f, 70f are negative, therefore, for a more clear illustration, the respective absolute values have been used.

represents the timeframe of action of a particular mode while the amplitude reflects the impact of the mode on the evolution of the system. In the current case, the timescale increase suggests that the particular mode requires more time to act and reach equilibrium, while the amplitude decrease indicates that its impact decreases. Consequently, the mode (in terms of amplitude and timescale) becomes less effective. These results are in agreement with a similar investigation for the effect of H_2O addition in methane/air mixtures [144], where an amplitude decrease and a timescale increase were reported after the addition of H_2O.

The system's decreased temperature that is achieved in the post ignition part of the process is probably the main mechanism that reduces the effect of the key reactions towards the formation of NO. But in fact there is another mechanism that holds. In particular, as it was reported in Ref. [144], the introduction of H_2O, affects the equilibration of the CSP (exhausted) mode that is associated with the O radical. The largest TPIs and APIs for this mode relate to reactions 7f and 7b (O + $H_2O \leftrightarrow$ 2OH), as shown in Fig. 28 which displays the CSP diagnostics for the 0- and 1-H_2O addition cases. Therefore, it is reasonable that the CSP Po identifies mostly O and in a much less degree OH, as the variables

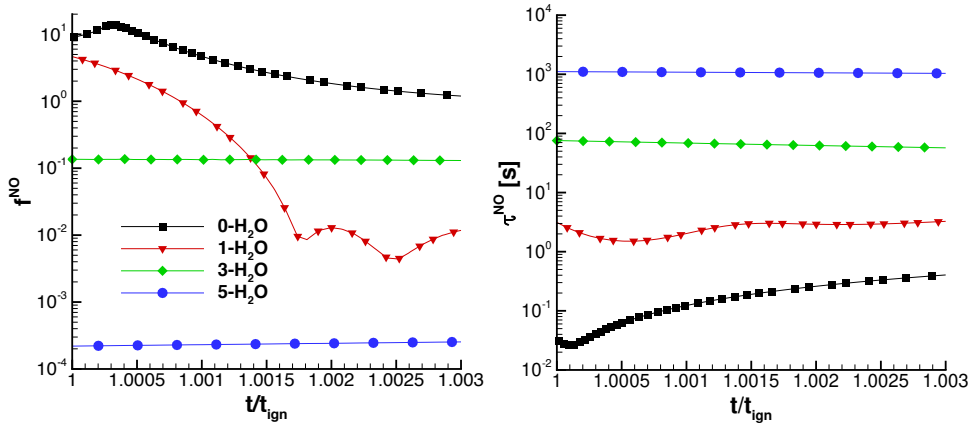

(a) (b)

Figure 27: The evolution of the amplitude (a) and the timescale (b) of the CSP mode that relates to the Y_{NO}, for the various H_2O addition cases, during the homogeneous adiabatic constant pressure autoignition of a 90%H_2-10%H_2O_2/air mixture at p(0)=40 atm, T(0)=900 K, $\phi = 0.4$.

720 mostly related to that mode. This mode becomes exhausted because of the equilibration of reaction 7. In Ref. [144] it was explained that in order for the equilibration of reaction 7f-7b to be maintained the O radicals decrease.

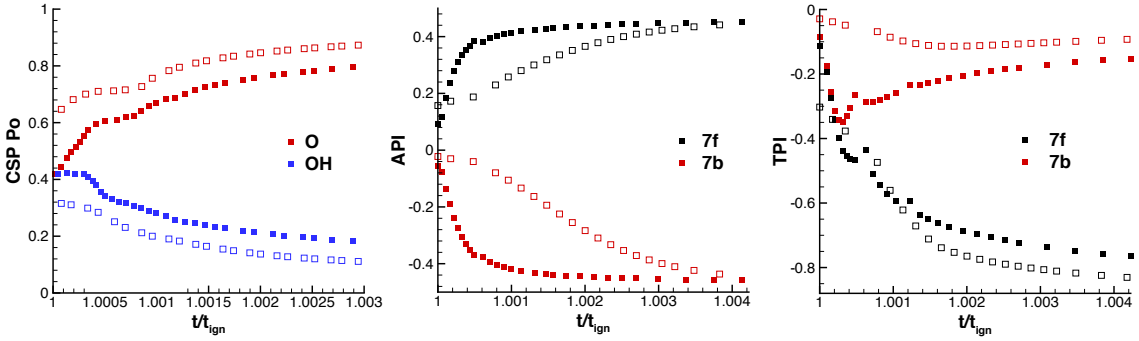

(a) (b) (c)

Figure 28: CSP diagnostics of the mode that relates to O in the post ignition area, for the 0% and 10% H_2O addition cases (hollow and blocked symbols, respectively), during the homogeneous adiabatic constant pressure autoignition of a 90%H_2-10%H_2O_2/air mixture at p(0)=40 atm, T(0)=900 K, $\phi = 0.4$.

The key chemical reactions that control the production of N_2O, remain

roughly the same, after the addition of H_2O, as depicted in Fig. 29, with two exceptions: reactions 3f and 5f become more important. In detail, the reaction pathway 7b-149b continues to be instrumental to the production of N_2O, after the addition of H_2O and 149b maintains the dominant role. However, its unscaled index drops roughly by an order of magnitude in the 1-H_2O case. Likewise, 7b, experiences a significant reduction of its related unscaled importance index and in fact, its scaled importance index remain very low in the early post ignition part. Similarly, reactions 7f and 149f which have the largest negative contributions in both cases, thus tend to decrease N_2O, both experience significant reductions in their scaled and unscaled importance indices with the addition of H_2O. In addition, reactions 3f and 5f (both hydrogen related), increase significantly their relative importance in the 1-H_2O case, thus, added up to the set of key reactions that control the evolution of N_2O. It is noted, however, that although their scaled indices increase after the addition of H_2O, their unscaled ones are still smaller or roughly equal to the 0-H_2O case, suggesting that they become important mainly because the absolute importances of the rest drops more than theirs. The key message is that with the addition of H_2O, N_2O production drops mainly because the 7b-149b pathway weakens, the weakening of 7b being more pronounced than 149b, thus other hydrogen-related reactions (3f and 5f) become more important to fill the gap for the required O atoms that are essential in 149b.

Finally, the examination of the CSP mode related to N_2O in Fig. 30, reveals that with H_2O addition the mode's amplitude decreases and the related timescale increase, in agreement with what was previously reported about NO, suggesting the related mode becomes less effective. The timescale increase indicates longer time required to reach equilibrium while the decreased amplitude demonstrates the decreased impact of that mode.

In summary:

- steam dilution induces a dramatic decrease to all NOx emissions and temperature in the post-ignition part.

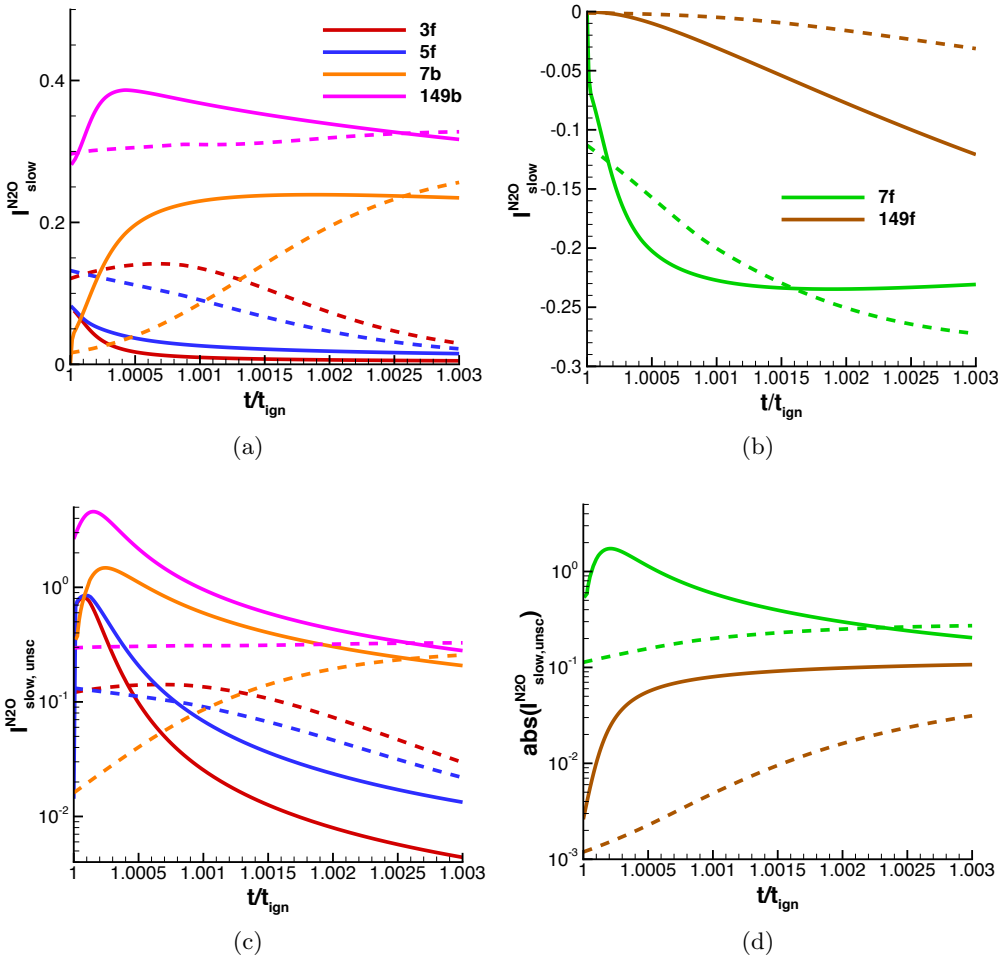

Figure 29: The largest scaled (a,b) and unscaled (c,d) slow Importance Indices for N_2O ($I^{N_2O}_{slow}$) for the 0- and 1- H_2O addition cases (solid and dashed lines, respectively), during the homogeneous adiabatic constant pressure autoignition of a 90%H_2-10%H_2O_2/air mixture at p(0)=40 atm, T(0)=900 K, $\phi = 0.4$. The indices related to reactions 7f, 149f are negative, therefore, for a more clear illustration, the absolute values of the unscaled importance indices were used.

- the NNH and thermal mechanisms both remain the key pathways that drive the formation of NO but their impact drops.

- with the addition of steam the timescale of the CSP mode related to

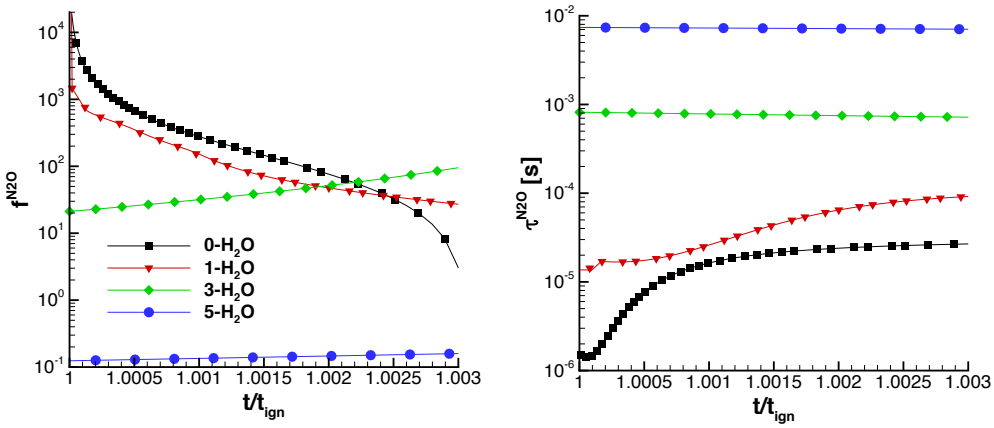

(a) (b)

Figure 30: The evolution of the amplitude (a) and the timescale (b) of the CSP mode that relates to the Y_{NO}, for the various H_2O addition cases, during the homogeneous adiabatic constant pressure autoignition of a 90%H_2-10%H_2O_2/air mixture at p(0)=40 atm, T(0)=900 K, $\phi = 0.4$.

NO increases while the associated amplitude drops, therefore, the mode becomes less effective.

- the decreased temperature is one of the two mechanisms that lead to the decreased impact of the NNH and thermal mechanisms for the production of NO, due to the steam dilution. The other relates to the shifting of the equilibration of the CSP (exhausted) mode that is associated with the O radical.

- the chemical pathway that controls the production of N_2O (reactions 7b and 149b) remains the same after the addition of steam, but its impact decreases.

- with the addition of steam the timescale of the CSP mode related to N_2O increases while the associated amplitude drops, therefore, the mode becomes less effective.

4. Conclusions

In the current work, the idea of using hydrogen peroxide as an additive in hydrogen/air mixtures was tested with the purpose of sufficiently promoting ignition, thus enabling the use of hydrogen in CI engines without relying on carbon-based fuels. The analysis highlighted that 5-10% H_2O_2 addition can be sufficient to accelerate ignition, achieving ignition delay times relevant to CI conditions. Not only that, but it was also found that the H_2O_2 addition tends to drop NO emissions significantly, reaching ∼98% decrease with 10% of H_2O_2 addition. However, a small increase of N_2O emissions was reported.

With respect to the changes in the key chemistry, it was reported that the addition of H_2O_2:

- decreases significantly the importance of reactions 11b ($H_2O_2 + H \leftarrow H_2 + HO_2$) and 19/20f ($2HO_2 \rightarrow H_2O_2 + O_2$) in controlling the ignition delay time; reaction 11b promoting and reaction 19/20f opposing ignition.
- increases the effect of reactions 9f (H_2O_2 (+M) $\rightarrow$ 2OH(+M)) and 3f ($H_2 + OH \rightarrow H_2O + H$) in controlling the ignition delay time; both reactions favoring ignition.
- increases the influence of temperature, becoming the key variable that controls the temporal evolution of the system, while that of H_2O_2 drops significantly.
- increases the contributions of reactions 5f ($H + O_2 \rightarrow OH + O$) and 21f ($H + O_2$ (+M) $\rightarrow$ HO_2 (+M)) to the temperature rate of change close to the inflection point (the former tends to decrease and the latter tends to increase temperature's rate of change), but 5f is favored more, thus decelerating the temperature increase. This has a great effect on NO production.
- decreases the influence of the thermal and NNH mechanisms, thus, resulting to lower NO values.

- increases the influence of reaction 149b (N_2O (+M) $\leftrightarrow$ N_2 + O (+M)) due to the increased pool of O radicals, thus leading to higher N_2O values.

Next, the addition of steam was tested as an efficient method for further reduction of NOx emissions. Firstly, it was reported that this approach has small effect on the ignition delay time, which tends to increase as the steam addition and/or initial temperature increase. Thus, up to ∼40% H_2O (by volume) addition to a 90% H_2-10% H_2O_2/air mixture results in ignition delay times which are relevant to CI engine operation. The small ignition delay time increase is accompanied by a significant reduction of the end (equilibrium) temperature. At sufficiently high steam addition (or/and as the initial temperature increases), a distinct two stage ignition process becomes evident. This unique phenomenon is important because it is the first time that a two stage ignition is reported on the basis of solely hydrogen based mixtures, with no inclusion of any carbon-based chemical species. The analysis revealed that the 2nd stage is created due to the increased influence of the chain termination reaction 18f (HO_2 + OH $\rightarrow$ H_2O + O_2) which tends to stop the ignition process by scavenging the HO_2 and OH radicals. Furthermore, steam addition was reported to induce a spectacular decrease of NO along with a significant decrease on the N_2O production. The key mechanisms that drive the formation of NO remain the same, i.e., the NNH and thermal (Zeldovich), however, they are significantly weakened when steam is added to the mixture. Also, the CSP mode related to NO was reported to have its amplitude decreased and its timescale increased; these findings explain further the notable NO decrease. The weakening of the NNH and thermal mechanisms is due to: (i) the decreased temperature reached in the post ignition part and (ii) the decrease of O radicals. Finally, the production of N_2O was reported to be due to the decreasing effect of reactions 7b (O + H_2 O $\leftrightarrow$ 2OH) - 149b (N_2O (+M) $\leftrightarrow$ N_2 + O (+M)).

In overall, the proposed technology using mixtures of hydrogen/hydrogen peroxide and steam, demonstrated a great potential for use in CI engine conditions. However, further studies are required that will showcase in more detail

the advantages of this technology. Also, the two stage ignition that was reported at sufficiently high steam addition conditions requires further investigation, as it was shown that this phenomenon becomes more pronounced at higher initial temperatures.

5. Acknowledgments

The current work has been supported by the Royal Society of Edinburgh (RSE) through the RSE/Scottish Government Sabbatical Research Grant scheme with grant no. 64676.

[1] G. Kalghatgi, Is it really the end of internal combustion engines and petroleum in transport?, Appl. Energy. 225 (2018) 965–974.

[2] W. Cecil, On the application of hydrogen gas to produce a moving power in machinery; with a description of an engine which is moved by the pressure of the atmosphere, upon a vacuum caused by explosions of hydrogen and atmospheric air, Trans. Cambridge Philos. Soc 1 (1822) 217.

[3] P. De Boer, W. McLean, H. Homan, Performance and emissions of hydrogen fueled internal combustion engines, Int. J. Hydrog. Energy 1 (2) (1976) 153–172.

[4] G. A. Karim, Hydrogen as a spark ignition engine fuel, Int. J. Hydrog. Energy 28 (5) (2003) 569–577.

[5] S. Verhelst, R. Sierens, S. Verstraeten, A critical review of experimental research on hydrogen fueled si engines, SAE Transactions 115 (2006) 264–274.

[6] C. White, R. Steeper, A. Lutz, The hydrogen-fueled internal combustion engine: a technical review, Int. J. Hydrog. Energy 31 (10) (2006) 1292–1305.

[7] S. Verhelst, Recent progress in the use of hydrogen as a fuel for internal combustion engines, Int. J. Hydrog. Energy 39 (2) (2014) 1071–1085.

[8] J. Naber, D. Siebers, Hydrogen combustion under diesel engine conditions, Int. J. Hydrog. Energy 23 (5) (1998) 363–371.

[9] H. A. Alrazen, A. A. Talib, R. Adnan, K. Ahmad, A review of the effect of hydrogen addition on the performance and emissions of the compression–ignition engine, Renew. Sust. Energ. Rev. 54 (2016) 785–796.

[10] V. Chintala, K. Subramanian, A comprehensive review on utilization of hydrogen in a compression ignition engine under dual fuel mode, Renew. Sust. Energ. Rev. 70 (2017) 472–491.

[11] P. Dimitriou, T. Tsujimura, A review of hydrogen as a compression ignition engine fuel, Int. J. Hydrog. Energy 42 (38) (2017) 24470–24486.

[12] M. Alias, A. Hairuddin, M. Hassan, K. Rezali, A review of hydrogen addition in an hcci engine fueled with biofuels, in: AIP Conference Proceedings, Vol. 2059, AIP Publishing LLC, 2019, p. 020045.

[13] N. Saravanan, G. Nagarajan, C. Dhanasekaran, K. M. Kalaiselvan, Experimental investigation of hydrogen fuel injection in di dual fuel diesel engine, in: SAE Tech. Pap., SAE International, 2007. doi:10.4271/2007-01-1465.
URL https://doi.org/10.4271/2007-01-1465

[14] B. H. Rao, K. Shrivastava, H. Bhakta, Hydrogen for dual fuel engine operation, Int. J. Hydrog. Energy 8 (5) (1983) 381–384.

[15] H. Mathur, L. Das, T. Patro, Hydrogen fuel utilization in ci engine powered end utility systems, Int. J. Hydrog. Energy 17 (5) (1992) 369–374.

[16] H. Mathur, L. Das, T. Patro, Hydrogen-fuelled diesel engine: performance improvement through charge dilution techniques, Int. J. Hydrog. Energy 18 (5) (1993) 421–431.

[17] G. Gopal, P. S. Rao, K. Gopalakrishnan, B. Murthy, Use of hydrogen in dual-fuel engines, Int. J. Hydrog. Energy 7 (3) (1982) 267–272.

[18] N. Saravanan, G. Nagarajan, C. Dhanasekaran, K. Kalaiselvan, Experimental investigation of hydrogen port fuel injection in di diesel engine, Int. J. Hydrog. Energy 32 (16) (2007) 4071–4080.

[19] N. Saravanan, G. Nagarajan, An experimental investigation of hydrogen-enriched air induction in a diesel engine system, Int. J. Hydrog. Energy 33 (6) (2008) 1769–1775.

[20] N. Saravanan, G. Nagarajan, K. Kalaiselvan, C. Dhanasekaran, An experimental investigation on hydrogen as a dual fuel for diesel engine system with exhaust gas recirculation technique, Renew. Energy 33 (3) (2008) 422–427.

[21] N. Saravanan, G. Nagarajan, S. Narayanasamy, An experimental investigation on di diesel engine with hydrogen fuel, Renew. Energy 33 (3) (2008) 415–421.

[22] M. M. Roy, E. Tomita, N. Kawahara, Y. Harada, A. Sakane, Performance and emission comparison of a supercharged dual-fuel engine fueled by producer gases with varying hydrogen content, Int. J. Hydrog. Energy 34 (18) (2009) 7811–7822.

[23] M. M. Roy, E. Tomita, N. Kawahara, Y. Harada, A. Sakane, An experimental investigation on engine performance and emissions of a supercharged h2-diesel dual-fuel engine, Int. J. Hydrog. Energy 35 (2) (2010) 844–853.

[24] G. K. Lilik, H. Zhang, J. M. Herreros, D. C. Haworth, A. L. Boehman, Hydrogen assisted diesel combustion, Int. J. Hydrog. Energy 35 (9) (2010) 4382–4398.

[25] C. Liew, H. Li, J. Nuszkowski, S. Liu, T. Gatts, R. Atkinson, N. Clark, An experimental investigation of the combustion process of a heavy-duty diesel engine enriched with h2, Int. J. Hydrog. Energy 35 (20) (2010) 11357–11365.

[26] B. Shin, Y. Cho, D. Han, S. Song, K. M. Chun, Investigation of the effects of hydrogen on cylinder pressure in a split-injection diesel engine at heavy egr, Int. J. Hydrog. Energy 36 (20) (2011) 13158–13170.

[27] T. Miyamoto, H. Hasegawa, M. Mikami, N. Kojima, H. Kabashima, Y. Urata, Effect of hydrogen addition to intake gas on combustion and exhaust emission characteristics of a diesel engine, Int. J. Hydrog. Energy 36 (20) (2011) 13138–13149.

[28] S. Liu, H. Li, C. Liew, T. Gatts, S. Wayne, B. Shade, N. Clark, An experimental investigation of no2 emission characteristics of a heavy-duty h2-diesel dual fuel engine, Int. J. Hydrog. Energy 36 (18) (2011) 12015–12024.

[29] A. Boretti, Advantages of the direct injection of both diesel and hydrogen in dual fuel h2ice, Int. J. Hydrog. Energy 36 (15) (2011) 9312–9317.

[30] V. SinghYadav, S. Soni, D. Sharma, Performance and emission studies of direct injection ci engine in duel fuel mode (hydrogen-diesel) with egr, Int. J. Hydrog. Energy 37 (4) (2012) 3807–3817.

[31] O. H. Ghazal, Performance and combustion characteristic of ci engine fueled with hydrogen enriched diesel, Int. J. Hydrog. Energy 38 (35) (2013) 15469–15476.

[32] V. S. Yadav, S. Soni, D. Sharma, Engine performance of optimized hydrogen-fueled direct injection engine, Energy 65 (2014) 116–122.

[33] V. Chintala, K. A. Subramanian, Assessment of maximum available work of a hydrogen fueled compression ignition engine using exergy analysis, Energy 67 (2014) 162–175.

[34] A. Maghbouli, W. Yang, H. An, S. Shafee, J. Li, S. Mohammadi, Modeling knocking combustion in hydrogen assisted compression ignition diesel engines, Energy 76 (2014) 768–779.

[35] M. Deb, A. Majumder, R. Banerjee, G. Sastry, P. Bose, A taguchi-fuzzy based multi-objective optimization study on the soot-nox-bthe characteristics of an existing ci engine under dual fuel operation with hydrogen, Int. J. Hydrog. Energy 39 (35) (2014) 20276–20293.

[36] A. Dhole, R. Yarasu, D. Lata, S. Baraskar, Mathematical modeling for the performance and emission parameters of dual fuel diesel engine using hydrogen as secondary fuel, Int. J. Hydrog. Energy 39 (24) (2014) 12991–13001.

[37] S.-R. Jhang, K.-S. Chen, S.-L. Lin, Y.-C. Lin, W. L. Cheng, Reducing pollutant emissions from a heavy-duty diesel engine by using hydrogen additions, Fuel 172 (2016) 89–95.

[38] M. O. Hamdan, M. Y. Selim, S.-A. Al-Omari, E. Elnajjar, Hydrogen supplement co-combustion with diesel in compression ignition engine, Renew. Energy 82 (2015) 54–60.

[39] V. S. Yadav, D. Sharma, S. Soni, Performance and combustion analysis of hydrogen-fuelled ci engine with egr, Int. J. Hydrog. Energy 40 (12) (2015) 4382–4391.

[40] M. Deb, P. Majumder, A. Majumder, S. Roy, R. Banerjee, Application of artificial intelligence (ai) in characterization of the performance–emission profile of a single cylinder ci engine operating with hydrogen in dual fuel mode: an ann approach with fuzzy-logic based topology optimization, Int. J. Hydrog. Energy 41 (32) (2016) 14330–14350.

[41] J. Zhou, C. Cheung, W. Zhao, C. Leung, Diesel–hydrogen dual-fuel combustion and its impact on unregulated gaseous emissions and particulate emissions under different engine loads and engine speeds, Energy 94 (2016) 110–123.

[42] V. Chintala, K. Subramanian, Cfd analysis on effect of localized in-cylinder temperature on nitric oxide (no) emission in a compression ig-

nition engine under hydrogen-diesel dual-fuel mode, Energy 116 (2016) 470–488.

[43] V. Chintala, K. Subramanian, Experimental investigation of autoignition of hydrogen-air charge in a compression ignition engine under dual-fuel mode, Energy 138 (2017) 197–209.

[44] H. Taghavifar, S. Anvari, A. Parvishi, Benchmarking of water injection in a hydrogen-fueled diesel engine to reduce emissions, Int. J. Hydrog. Energy 42 (16) (2017) 11962–11975.

[45] M. Talibi, P. Hellier, N. Ladommatos, The effect of varying egr and intake air boost on hydrogen-diesel co-combustion in ci engines, Int. J. Hydrog. Energy 42 (9) (2017) 6369–6383.

[46] A. Çalık, Determination of vibration characteristics of a compression ignition engine operated by hydrogen enriched diesel and biodiesel fuels, Fuel 230 (2018) 355–358.

[47] P. Dimitriou, M. Kumar, T. Tsujimura, Y. Suzuki, Combustion and emission characteristics of a hydrogen-diesel dual-fuel engine, Int. J. Hydrog. Energy 43 (29) (2018) 13605–13617.

[48] J. Serrano, F. Jiménez-Espadafor, A. López, Analysis of the effect of different hydrogen/diesel ratios on the performance and emissions of a modified compression ignition engine under dual-fuel mode with water injection. hydrogen-diesel dual-fuel mode, Energy 172 (2019) 702–711.

[49] J. Serrano, F. Jiménez-Espadafor, A. López, Analysis of the effect of the hydrogen as main fuel on the performance of a modified compression ignition engine with water injection, Energy 173 (2019) 911–925.

[50] A. I. Jabbr, U. O. Koylu, Influence of operating parameters on performance and emissions for a compression-ignition engine fueled by hydrogen/diesel mixtures, Int. J. Hydrog. Energy 44 (26) (2019) 13964–13973.

[51] S. Nag, P. Sharma, A. Gupta, A. Dhar, Experimental study of engine performance and emissions for hydrogen diesel dual fuel engine with exhaust gas recirculation, Int. J. Hydrog. Energy 44 (23) (2019) 12163–12175.

[52] H. T. Arat, Simulation of diesel hybrid electric vehicle containing hydrogen enriched ci engine, Int. J. Hydrog. Energy 44 (20) (2019) 10139–10146.

[53] T. Tsujimura, Y. Suzuki, The utilization of hydrogen in hydrogen/diesel dual fuel engine, Int. J. Hydrog. Energy 42 (19) (2017) 14019–14029.

[54] J. Syed, R. U. Baig, S. Algarni, Y. S. Murthy, M. Masood, M. Inamurrahman, Artificial neural network modeling of a hydrogen dual fueled diesel engine characteristics: An experiment approach, Int. J. Hydrog. Energy 42 (21) (2017) 14750–14774.

[55] L. Li, Y. Yu, W. Lin, Numerical investigation on the effects of load conditions and hydrogen-air ratio on the combustion processes of a hsdi engine, Int. J. Hydrog. Energy 45 (17) (2020) 10602–10612.

[56] T. Korakianitis, A. Namasivayam, R. Crookes, Hydrogen dual-fuelling of compression ignition engines with emulsified biodiesel as pilot fuel, Int. J. Hydrog. Energy 35 (24) (2010) 13329–13344.

[57] H. An, W. Yang, A. Maghbouli, J. Li, S. Chou, K. J. Chua, J. Wang, L. Li, Numerical investigation on the combustion and emission characteristics of a hydrogen assisted biodiesel combustion in a diesel engine, Fuel 120 (2014) 186–194.

[58] M. A. Rahman, A. Ruhul, M. Aziz, R. Ahmed, Experimental exploration of hydrogen enrichment in a dual fuel ci engine with exhaust gas recirculation, Int. J. Hydrog. Energy 42 (8) (2017) 5400–5409.

[59] M. T. Chaichan, Performance and emission characteristics of cie using hydrogen, biodiesel, and massive egr, Int. J. Hydrog. Energy 43 (10) (2018) 5415–5435.

[60] P. Dimitriou, T. Tsujimura, Y. Suzuki, Adopting biodiesel as an indirect way to reduce the nox emission of a hydrogen fumigated dual-fuel engine, Fuel 244 (2019) 324–334.

[61] M. Aldhaidhawi, R. Chiriac, V. Bădescu, G. Descombes, P. Podevin, Investigation on the mixture formation, combustion characteristics and performance of a diesel engine fueled with diesel, biodiesel b20 and hydrogen addition, Int. J. Hydrog. Energy 42 (26) (2017) 16793–16807.

[62] M. A. Akar, E. Kekilli, O. Bas, S. Yildizhan, H. Serin, M. Ozcanli, Hydrogen enriched waste oil biodiesel usage in compression ignition engine, Int. J. Hydrog. Energy 43 (38) (2018) 18046–18052.

[63] M. R. A. Mansor, M. M. Abbood, T. I. Mohamad, The influence of varying hydrogen-methane-diesel mixture ratio on the combustion characteristics and emissions of a direct injection diesel engine, Fuel 190 (2017) 281–291.

[64] S. Karimkashi, H. Kahila, O. Kaario, M. Larmi, V. Vuorinen, Numerical study on tri-fuel combustion: Ignition properties of hydrogen-enriched methane-diesel and methanol-diesel mixtures, Int. J. Hydrog. Energy 45 (7) (2020) 4946–4962.

[65] L. Tarabet, M. Lounici, K. Loubar, K. Khiari, R. Bouguessa, M. Tazerout, Hydrogen supplemented natural gas effect on a di diesel engine operating under dual fuel mode with a biodiesel pilot fuel, Int. J. Hydrog. Energy 43 (11) (2018) 5961–5971.

[66] W. Tutak, A. Jamrozik, K. Grab-Rogaliński, Effect of natural gas enrichment with hydrogen on combustion process and emission characteristic of a dual fuel diesel engine, Int. J. Hydrog. Energy 45 (15) (2020) 9088–9097.

[67] M. Parthasarathy, J. I. J. Lalvani, B. Dhinesh, K. Annamalai, Effect of hydrogen on ethanol–biodiesel blend on performance and emission characteristics of a direct injection diesel engine, Ecotoxicol. Environ. Saf. 134 (2016) 433–439.

[68] E. Sukjit, J. M. Herreros, K. Dearn, A. Tsolakis, K. Theinnoi, Effect of hydrogen on butanol–biodiesel blends in compression ignition engines, Int. J. Hydrog. Energy 38 (3) (2013) 1624–1635.

[69] C. Rakopoulos, M. Scott, D. Kyritsis, E. Giakoumis, Availability analysis of hydrogen/natural gas blends combustion in internal combustion engines, Energy 33 (2) (2008) 248–255.

[70] S. Imran, D. Emberson, B. Ihracska, D. Wen, R. Crookes, T. Korakianitis, Effect of pilot fuel quantity and type on performance and emissions of natural gas and hydrogen based combustion in a compression ignition engine, Int. J. Hydrog. Energy 39 (10) (2014) 5163–5175.

[71] N. Saravanan, G. Nagarajan, G. Sanjay, C. Dhanasekaran, K. Kalaiselvan, Combustion analysis on a di diesel engine with hydrogen in dual fuel mode, Fuel 87 (17-18) (2008) 3591–3599.

[72] M. S. Kumar, A. Ramesh, B. Nagalingam, Use of hydrogen to enhance the performance of a vegetable oil fuelled compression ignition engine, Int. J. Hydrog. Energy 28 (10) (2003) 1143–1154.

[73] S. Verma, A. Suman, L. Das, S. Kaushik, S. Tyagi, A renewable pathway towards increased utilization of hydrogen in diesel engines, Int. J. Hydrog. Energy 45 (8) (2020) 5577–5587.

[74] S. Halewadimath, V. Yaliwal, N. Banapurmath, A. Sajjan, Influence of hydrogen enriched producer gas (hpg) on the combustion characteristics of a crdi diesel engine operated on dual-fuel mode using renewable and sustainable fuels, Fuel 270 (2020) 117575.

[75] N. Hariharan, V. Senthil, M. Krishnamoorthi, S. Karthic, Application of artificial neural network and response surface methodology for predicting and optimizing dual-fuel ci engine characteristics using hydrogen and bio fuel with water injection, Fuel 270 (2020) 117576.

[76] D. Lata, A. Misra, Theoretical and experimental investigations on the performance of dual fuel diesel engine with hydrogen and lpg as secondary fuels, Int. J. Hydrog. Energy 35 (21) (2010) 11918–11931.

[77] D. Lata, A. Misra, Analysis of ignition delay period of a dual fuel diesel engine with hydrogen and lpg as secondary fuels, Int. J. Hydrog. Energy 36 (5) (2011) 3746–3756.

[78] D. Lata, A. Misra, S. Medhekar, Investigations on the combustion parameters of a dual fuel diesel engine with hydrogen and lpg as secondary fuels, Int. J. Hydrog. Energy 36 (21) (2011) 13808–13819.

[79] D. Lata, A. Misra, S. Medhekar, Effect of hydrogen and lpg addition on the efficiency and emissions of a dual fuel diesel engine, Int. J. Hydrog. Energy 37 (7) (2012) 6084–6096.

[80] K. Pichayapat, S. Sukchai, S. Thongsan, A. Pongtornkulpanich, Emission characteristics of using hcng in the internal combustion engine with minimum pilot diesel injection for greater fuel economy, Int. J. Hydrog. Energy 39 (23) (2014) 12182–12186.

[81] N. Khatri, K. K. Khatri, Hydrogen enrichment on diesel engine with biogas in dual fuel mode, Int. J. Hydrog. Energy 45 (11) (2020) 7128–7140.

[82] A. S. Bika, L. M. Franklin, D. B. Kittelson, Hydrogen as a combustion modifier of ethanol in compression ignition engines, in: SAE Tech. Pap., SAE International, 2009.

[83] H. Homan, R. Reynolds, P. De Boer, W. McLean, Hydrogen-fueled diesel engine without timed ignition, Int. J. Hydrog. Energy 4 (4) (1979) 315–325.

[84] A. Welch, J. Wallace, Performance characteristics of a hydrogen-fueled diesel engine with ignition assist, in: SAE Tech. Pap., SAE International, 1990.

[85] J. G. Antunes, R. Mikalsen, A. Roskilly, An experimental study of a direct injection compression ignition hydrogen engine, Int. J. Hydrog. Energy 34 (15) (2009) 6516–6522.

[86] A. Boretti, A. Osman, I. Aris, Direct injection of hydrogen, oxygen and water in a novel two stroke engine, Int. J. Hydrog. Energy 36 (16) (2011) 10100–10106.

[87] A. Boretti, Advances in hydrogen compression ignition internal combustion engines, Int. J. Hydrog. Energy 36 (19) (2011) 12601–12606.

[88] R. Kavtaradze, T. Natriashvili, S. Gladyshev, Hydrogen-diesel engine: Problems and prospects of improving the working process, in: SAE Tech. Pap., SAE International, 2019.

[89] S. Fukuzumi, Y. Yamada, K. D. Karlin, Hydrogen peroxide as a sustainable energy carrier: electrocatalytic production of hydrogen peroxide and the fuel cell, Electrochim. Acta 82 (2012) 493–511.

[90] R. Amri, T. Rezoug, Numerical study of liquid propellants combustion for space applications, Acta Astronaut. 69 (7-8) (2011) 485–498.

[91] R. Amri, D. Gibbon, T. Rezoug, The design, development and test of one newton hydrogen peroxide monopropellant thruster, Aerosp. Sci. Technol. 25 (1) (2013) 266–272.

[92] A. Okninski, J. Kindracki, P. Wolanski, Multidisciplinary optimisation of bipropellant rocket engines using h2o2 as oxidiser, Aerosp. Sci. Technol. 82 (2018) 284–293.

[93] J.-Y. Lestrade, J. Anthoine, A. J. Musker, A. Lecossais, Experimental demonstration of an end-burning swirling flow hybrid rocket engine, Aerosp. Sci. Technol. 92 (2019) 1–8.

[94] B. L. Austin, S. Heister, W. Anderson, Characterization of pintle engine performance for nontoxic hypergolic bipropellants, J. Propuls. Power 21 (4) (2005) 627–635.

[95] L. Casalino, D. Pastrone, Oxidizer control and optimal design of hybrid rockets for small satellites, J. Propuls. Power 21 (2) (2005) 230–238.

[96] L. Casalino, D. Pastrone, Optimal design of hybrid rocket motors for launchers upper stages, J. Propuls. Power 26 (3) (2010) 421–427.

[97] G. Glivin, V. Sreeja, Development of hydrogen peroxide based propellant systems for increasing energy efficiency, in: 2019 International Conference on Recent Advances in Energy-efficient Computing and Communication (ICRAECC), IEEE, 2019, pp. 1–4.

[98] W. Hertzelle, M. Waite, Design of a small h2o2/htpb hybrid sounding rocket motor, in: 34th Aerospace Sciences Meeting and Exhibit, 1996, p. 8.

[99] T. Jacks, M. Beisler, Expanding hydrogen peroxide propulsion test capability at nasa's stennis space center e-complex, in: 39th AIAA/ASME/SAE/ASEE Joint Propulsion Conference and Exhibit, 2003, p. 5041.

[100] B. Gribi, Y. Lin, X. Hui, C. Zhang, C.-J. Sung, Effects of hydrogen peroxide addition on combustion characteristics of n-decane/air mixtures, Fuel 223 (2018) 324–333.

[101] M. H. Morsy, Ignition control of methane fueled homogeneous charge compression ignition engines using additives, Fuel 86 (4) (2007) 533–540.

[102] M. H. Morsy, Modeling study on the production of hydrogen/syngas via partial oxidation using a homogeneous charge compression ignition engine fueled with natural gas, Int. J. Hydrog. Energy 39 (2) (2014) 1096–1104.

[103] A. Noorpoor, M. Ghaffarpour, M. Aghsaee, A. Hamedani, Effects of fuel additives on ignition timing of methane fuelled hcci engine, J. Energy Inst. 82 (1) (2009) 37–42.

[104] Z. M. Hammond, J. H. Mack, R. W. Dibble, Effect of hydrogen peroxide addition to methane fueled homogeneous charge compression ignition engines through numerical simulations, Int. J. Engine Res. 17 (2) (2016) 209–220.

[105] D. M. Manias, E. A. Tingas, C. E. Frouzakis, K. Boulouchos, D. A. Goussis, The mechanism by which CH_2O and H_2O_2 additives affect the autoignition of CH_4/air mixtures, Combust. Flame 164 (2016) 111–125.

[106] C. Born, N. Peters, Reduction of soot emission at a di diesel engine by additional injection of hydrogen peroxide during combustion, in: SAE Tech. Pap., SAE International, 1998. doi:10.4271/982676.

[107] B. Fanz, P. Roth, Injection of a h2o2/water solution into the combustion chamber of a direct injection diesel engine and its effect on soot removal, Proc. Combust. Inst. 28 (1) (2000) 1219–1225.

[108] K. A. Subramanian, A. Ramesh, Use of hydrogen peroxide to improve the performance and reduce emissions of a ci engine fuelled with water diesel emulsions, in: SAE Tech. Pap., SAE International, 2008.

[109] M. Ashok, C. Saravanan, Role of hydrogen peroxide in a selected emulsified fuel ratio and comparing it to diesel fuel, Energ. Fuels 22 (3) (2008) 2099–2103.

[110] A. Demirci, H. Koten, M. Gumus, The effects of small amount of hydrogen addition on performance and emissions of a direct injection compression ignition engine, Therm. Sci. 22 (3) (2018) 1395–1404.

[111] J.-K. Yeom, S.-H. Jung, J.-H. Yoon, An experimental study on the application of oxygenated fuel to diesel engines, Fuel 248 (2019) 262–277.

[112] B. M. Krishna, Experimental investigation on ci engine with hydrogen peroxide as an alternate, Global Journal of Research In Engineering 20 (1). URL https://engineeringresearch.org/index.php/GJRE/article/view/2004

[113] R. Adnan, Z. S. Adlan, F. Munir, M. Asnawi, Experimental study on the effect of intake air temperature on the performance of spark ignition engine fueled with hydrogen peroxide, Stroke 2000 (2006) 66.

[114] Y. Wang, L. Wei, M. Yao, A theoretical investigation of the effects of the low-temperature reforming products on the combustion of n-heptane in an hcci engine and a constant volume vessel, Appl. Energy. 181 (2016) 132–139.

[115] M. C. Mulenga, D. S.-K. Ting, G. T. Reader, M. Zheng, The potential for reducing co and nox emissions from an hcci engine using h2o2 addition, in: SAE Tech. Pap., SAE International, 2003.

[116] K.-B. Nguyen, T. Dan, I. Asano, Combustion, performance and emission characteristics of direct injection diesel engine fueled by jatropha hydrogen peroxide emulsion, Energy 74 (2014) 301–308.

[117] A. Zhou, C. Zhang, Y. Li, S. Li, P. Yin, Effect of hydrogen peroxide additive on the combustion and emission characteristics of an n-butanol homogeneous charge compression ignition engine, Energy 169 (2019) 572–579.

[118] T. Li, J. Deng, T. T. Bao, Z. J. Wu, Numerical study on effect of hydrogen peroxide additive on ethanol hcci engine, in: Advanced Materials Research, Vol. 433, Trans Tech Publ, 2012, pp. 244–250.

[119] E. A. Tingas, D. C. Kyritsis, D. A. Goussis, Ignition delay control of DME/air and EtOH/air homogeneous autoignition with the use of various additives, Fuel 169 (2016) 15–24.

[120] M. Ashok, Identification of best additive using the selected ratio of ethanol–diesel-based emulsified fuel, Int. J. Sustain. Energy 31 (3) (2012) 203–212.

[121] A. T. Khalil, D. M. Manias, E.-A. Tingas, D. C. Kyritsis, D. A. Goussis, Algorithmic analysis of chemical dynamics of the autoignition of nh3–h2o2/air mixtures, Energies 12 (23) (2019) 4422.

[122] S. H. Lam, D. A. Goussis, Understanding complex chemical kinetics with Computational Singular Perturbation, Proc. Combust. Inst. 22 (1989) 931–941.

[123] C.-W. Zhou, Y. Li, U. Burke, C. Banyon, K. P. Somers, S. Ding, S. Khan, J. W. Hargis, T. Sikes, O. Mathieu, et al., An experimental and chemical kinetic modeling study of 1, 3-butadiene combustion: Ignition delay time and laminar flame speed measurements, Combust. Flame 197 (2018) 423–438.

[124] P. Glarborg, J. A. Miller, B. Ruscic, S. J. Klippenstein, Modeling nitrogen chemistry in combustion, Prog. Energ. Combust. 67 (2018) 31–68.

[125] S. H. Lam, D. A. Goussis, Conventional asymptotics and Computational Singular Perturbation for simplified kinetics modelling, in: M. O. Smooke (Ed.), Reduced kinetic mechanisms and asymptotic approximations for methane-air flames, no. 384 in Springer Lecture Notes, Springer-Verlag, Berlin, 1991, pp. 227–242.

[126] S. H. Lam, D. A. Goussis, CSP method for simplifying kinetics, Int. J. Chem. Kinet. 26 (4) (1994) 461–486.

[127] D. Goussis, U. Maas, Model reduction for combustion chemistry, in: T. Echekki, N. Mastorakos (Eds.), Turbulent Combustion Modeling, Fluid Mechanics and its Applications, Springer London, 2011, pp. 193–220.

[128] M. Valorani, F. Creta, P. Ciottoli, R. M. Galassi, D. Goussis, H. Najm, S. Paolucci, H. G. Im, E.-A. Tingas, D. Manias, et al., Computational singular perturbation method and tangential stretching rate analysis of large scale simulations of reactive flows: Feature tracking, time scale characterization, and cause/effect identification. part 1, basic concepts, in: Data

analysis for direct numerical simulations of turbulent combustion, Springer International Publishing, 2020, pp. 43–64.

[129] D. A. Goussis, H. N. Najm, Model reduction and physical understanding of slowly oscillating processes: The circadian cycle, Multiscale Model. Simul. 5 (2006) 1297–1332.

[130] D. J. Diamantis, D. C. Kyritsis, D. A. Goussis, The reactions favoring or opposing the development of explosive modes: auto-ignition of a homogeneous methane/air mixture, Proc. Combust. Inst. 35 (2015) 267–274.

[131] K. K. Yalamanchi, E.-A. Tingas, H. G. Im, S. M. Sarathy, Screening gas-phase chemical kinetic models: Collision limit compliance and ultrafast timescales, Int. J. Chem. Kinet. 52 (9) (2020) 599–610. arXiv: https://onlinelibrary.wiley.com/doi/pdf/10.1002/kin.21373, doi:10.1002/kin.21373.
URL https://onlinelibrary.wiley.com/doi/abs/10.1002/kin.21373

[132] Y. Li, A. Alfazazi, B. Mohan, E. A. Tingas, J. Badra, H. G. Im, S. M. Sarathy, Development of a reduced four-component (toluene/n-heptane/iso-octane/ethanol) gasoline surrogate model, Fuel 247 (2019) 164–178.

[133] D. J. Diamantis, E. Mastorakos, D. A. Goussis, H_2/air autoignition: The nature and interaction of the developing explosive modes, Combust. Theor. Model. 19 (2015) 382–433.

[134] E. Singh, E.-A. Tingas, D. Goussis, H. G. Im, S. M. Sarathy, Chemical ignition characteristics of ethanol blending with primary reference fuels, Energ. Fuel. 33 (10) (2019) 10185–10196.

[135] E.-A. Tingas, D. C. Kyritsis, D. A. Goussis, H 2/air autoignition dynamics around the third explosion limit, J. Energy Eng. 145 (1) (2019) 04018074.

[136] S. M. Sarathy, E.-A. Tingas, E. F. Nasir, A. Detogni, Z. Wang, A. Farooq, H. Im, Three-stage heat release in n-heptane auto-ignition, Proc. Combust. Inst. 37 (1) (2019) 485–492.

[137] W. Song, E.-A. Tingas, H. G. Im, A computational analysis of methanol autoignition enhancement by dimethyl ether addition in a counterflow mixing layer, Combust. Flame 195 (2018) 84–98.

[138] E. A. Tingas, D. M. Manias, S. M. Sarathy, D. A. Goussis, Ch4/air homogeneous autoignition: A comparison of two chemical kinetics mechanisms, Fuel 223 (2018) 74–85.

[139] E. A. Tingas, H. G. Im, D. C. Kyritsis, D. A. Goussis, The use of co2 as an additive for ignition delay and pollutant control in ch4/air autoignition, Fuel 211 (2018) 898–905.

[140] M. Hadjinicolaou, D. A. Goussis, Asymptotic solution of stiff PDEs with the CSP method: the reaction diffusion equation, SIAM J. SCI. COMPUT. 20 (1998) 781–810.

[141] D. A. Goussis, M. Valorani, F. Creta, H. N. Najm, Reactive and reactive-diffusive time scales in stiff reaction-diffusion systems, Prog. Comput. Fluid Dy. 5 (6) (2005) 316–326.

[142] M. Valorani, F. Creta, P. Ciottoli, R. M. Galassi, D. Goussis, H. Najm, S. Paolucci, H. G. Im, E.-A. Tingas, D. Manias, et al., Computational singular perturbation method and tangential stretching rate analysis of large scale simulations of reactive flows: Feature tracking, time scale characterization, and cause/effect identification. part 2, analyses of ignition systems, laminar and turbulent flames, in: Data analysis for direct numerical simulations of turbulent combustion, Springer International Publishing, 2020, pp. 65–88.

[143] D. G. Patsatzis, E.-A. Tingas, D. A. Goussis, S. M. Sarathy, Computa-

tional singular perturbation analysis of brain lactate metabolism, PloS one 14 (12) (2019) e0226094.

[144] E. A. Tingas, D. C. Kyritsis, D. A. Goussis, Algorithmic determination of the mechanism through which H_2O-dilution affects autoignition dynamics and NO formation in CH_4/air mixtures, Fuel 183 (2016) 90–98.

[145] D. M. Manias, E.-A. Tingas, Y. Minamoto, H. G. Im, Topological and chemical characteristics of turbulent flames at mild conditions, Combust. Flame 208 (2019) 86–98.

[146] D. M. Manias, E.-A. Tingas, F. E. H. Pérez, R. M. Galassi, P. P. Ciottoli, M. Valorani, H. G. Im, Investigation of the turbulent flame structure and topology at different karlovitz numbers using the tangential stretching rate index, Combust. Flame 200 (2019) 155–167.

[147] D. M. Manias, A.-E. Tingas, H. G. Im, Y. Minamoto, Dynamics analysis of a turbulent methane flame in mild combustion conditions, in: AIAA Scitech Forum, 2019, p. 1731.

[148] D. Manias, A.-E. Tingas, F. E. Hernandez Perez, H. G. Im, R. M. Galassi, P. P. Ciottoli, M. Valorani, Analysis of hydrogen/air turbulent premixed flames at different karlovitz numbers using computational singular perturbation, in: AIAA Aerospace Sciences Meeting, 2018, p. 0364.

[149] F. E. Hernandez Perez, H. G. Im, A. E. Tingas, Computational investigation of rod-stabilized laminar premixed hydrogen–methane–air flames, in: AIAA Scitech Forum, 2020, p. 1659.

[150] E. A. Tingas, D. C. Kyritsis, D. A. Goussis, Autoignition dynamics of DME/air and EtOH/air homogeneous mixtures, Combust. Flame 162 (9) (2015) 3263–3276.

[151] A. Massias, D. Diamantis, E. Mastorakos, D. Goussis, An algorithm for the construction of global reduced mechanisms with csp data, Combust. Flame 117 (4) (1999) 685–708.

[152] A. Massias, D. Diamantis, E. Mastorakos, D. Goussis, Global reduced mechanisms for methane and hydrogen combustion with nitric oxide formation constructed with csp data, Combustion theory and modelling 3 (2) (1999) 233–257.

[153] E.-A. Tingas, D. J. Diamantis, D. A. Goussis, Issues arising in the construction of qssa mechanisms: the case of reduced n-heptane/air models for premixed flames, Combust. Theor. Model. 22 (6) (2018) 1049–1083.

[154] M. Jaasim, E.-A. Tingas, F. E. H. Pérez, H. G. Im, Computational singular perturbation analysis of super-knock in si engines, Fuel 225 (2018) 184–191.

[155] E.-A. Tingas, Z. Wang, S. M. Sarathy, H. G. Im, D. A. Goussis, Chemical kinetic insights into the ignition dynamics of n-hexane, Combust. Flame 188 (2018) 28–40.

[156] E.-A. Tingas, D. C. Kyritsis, D. A. Goussis, Comparative investigation of homogeneous autoignition of DME/air and EtOH/air mixtures at low initial temperatures, Combust. Theor. Model. 21 (1) (2017) 93–119.

[157] M. Valorani, F. Creta, D. A. Goussis, J. C. Lee, H. N. Najm, An automatic procedure for the simplification of chemical kinetic mechanisms based on csp, Combust. Flame 146 (1-2) (2006) 29–51.

[158] M. Valorani, F. Creta, F. Donato, H. N. Najm, D. A. Goussis, Skeletal mechanism generation and analysis for n-heptane with csp, Proc. Combust. Inst. 31 (1) (2007) 483–490.

[159] N. Sharmin, E.-A. Tingas, Dynamics analysis of a jet-fuel surrogate and development of a skeletal mechanism for computational fluid dynamic applications, J. Energy Eng. 146 (6) (2020) 04020064.

[160] S. Gupta, H. G. Im, M. Valorani, Classification of ignition regimes in HCCI combustion using computational singular perturbation, Proc. Combust. Inst. 33 (2) (2011) 2991–2999.

[161] S. Gupta, H. G. Im, M. Valorani, Analysis of n-heptane auto-ignition characteristics using computational singular perturbation, Proc. Combust. Inst. 34 (1) (2013) 1125–1133.

[162] P. Pal, M. Valorani, P. G. Arias, H. G. Im, M. S. Wooldridge, P. P. Ciottoli, R. M. Galassi, Computational characterization of ignition regimes in a syngas/air mixture with temperature fluctuations, Proc. Combust. Inst. 36 (3) (2017) 3705–3716.

[163] H. N. Najm, M. Valorani, D. A. Goussis, J. Prager, Analysis of methane–air edge flame structure, Combust. Theor. Model. 14 (2) (2010) 257–294.

[164] J. Prager, H. N. Najm, M. Valorani, D. Goussis, Structure of n-heptane/air triple flames in partially-premixed mixing layers, Combust. Flame 158 (11) (2011) 2128–2144.

[165] A. CHEMKIN-PRO, 18.0, ANSYS Reaction Design: San Diego.

[166] CSPTk - a software toolkit for the CSP and TSR analysis of kinetic models and the simplification and reduction of chemical kinetics mechanisms. The software can be obtained upon request to M.Valorani (mauro.valorani@uniroma1.it), Tech. rep., Sapienza University of Rome, Italy (2015).

[167] C. Safta, H. N. Najm, O. Knio, TChem-a software toolkit for the analysis of complex kinetic models, Sandia Report, SAND2011-3282.

[168] M. Valorani, P. P. Ciottoli, R. M. Galassi, S. Paolucci, T. Grenga, E. Martelli, Enhancements of the g-scheme framework, Flow Turbul. Combust. 101 (4) (2018) 1023–1033.

[169] R. Thompson, L. Lassaletta, P. Patra, C. Wilson, K. Wells, A. Gressent, E. Koffi, M. Chipperfield, W. Winiwarter, E. Davidson, et al., Acceleration of global n2o emissions seen from two decades of atmospheric inversion, Nat. Clim. Chang. 9 (12) (2019) 993–998.

[170] M. Morsy, S. Chung, Effect of additives on ignition of methane at homogeneous charge compression ignition engine-like conditions, Proc. Inst. Mech. Eng. D 221 (5) (2007) 605–619.

[171] D. S.-K. Ting, G. T. Reader, Hydrogen peroxide for improving premixed methane–air combustion, Energy 30 (2-4) (2005) 313–322.

[172] J. Zeldovich, The oxidation of nitrogen in combustion and explosions: Acta, In Physiochem.

[173] J. W. Bozzelli, A. M. Dean, O+NNH: A possible new route for NOx formation in flames, Int. J. Chem. Kinet. 27 (11) (1995) 1097–1109.

[174] P. Malte, D. Pratt, Measurement of atomic oxygen and nitrogen oxides in jet-stirred combustion, in: Proc. Combust. Inst., Vol. 15, Elsevier, 1975, pp. 1061–1070.